RICE UNIVERSITY

Electron correlation in extended systems *via* quantum embedding

by

Ireneusz W. Bulik

A THESIS SUBMITTED
IN PARTIAL FULFILLMENT OF THE
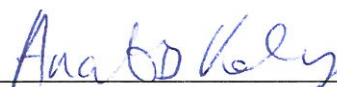REQUIREMENTS FOR THE DEGREE
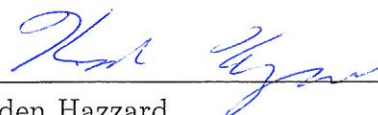
Doctor of Philosophy

APPROVED, THESIS COMMITTEE:

_____

Gustavo E. Scuseria, Chair
Robert A. Welch Professor of Chemistry;
Professor of Physics and Astronomy and
Materials Science and Nanomaterials
Engineering

_____

Anatoly Kolomeisky
Professor of Chemistry and Professor of
Chemical and Biomolecular Engineering

_____

Kaden Hazzard
Assistant Professor of Physics

_____

Houston, Texas

May, 2015

ABSTRACT

Electron correlation in extended systems *via* quantum embedding

by

Ireneusz W. Bulik

The pursuit of accurate and computationally efficient many-body tools capable of describing electron correlation is a major effort of the quantum chemistry community. The accuracy of chemical predictions strongly depends on the ability of the models to account for electron correlation. As the computational demand scales unfavourably with the size of the system, an efficient way of identifying relevant degrees of freedom may be an interesting avenue.

In this thesis, a quantum embedding approach is employed to study lattice systems, polymers, and crystals. Numerical data shows the accuracy of the quantum embedding theory when combined with high-level many-body techniques. As the size of the units that are embedded grows, a more approximate and more computationally affordable tools are called for. In this thesis, we investigate the possibility of forming such methods in the framework of coupled cluster theory.

We believe that the tools presented in this thesis could be important for accurate treatment of electron correlation in applications to realistic materials.

Acknowledgements

I would like to thank my advisor, Professor Gustavo E. Scuseria, for guidance over the entire period of my doctoral studies. The highly collaborative environment of his research group was extremely helpful and stimulating. In particular, discussions with Dr. Carlos Jimenéz-Hoyos, Dr. Rayner Roberto Rodríguez Guzmán and Dr. Matthias Degroote are kindly acknowledged. Finally, I am grateful to Dr. Thomas M. Henderson for guiding a simple Pole over a complex plane.

I would also like to thank my wife, Fangfang Wen for her support during my graduate education.

Contents

Illustrations

Tables

Chapter 1

Introduction

1.1 The electronic Schrödinger equation and chemistry

The collective goal of the quantum chemistry community is to provide computationally affordable and accurate predictions for chemical systems. It is only in the last century that we have known that all the quantities of chemical interest are built of electrons and nuclei. The chemical reactivity and stability of materials is governed by the movement of electrons in the electric field of the nuclei. Being able to properly describe the behavior of the electrons would allow one, in principle, to accurately explain not only chemical reactivity but also spectroscopic properties of materials. Moreover, the description of the nuclei in the field of electrons gives us a well defined way to predict, for example, vibrational spectra.

With the birth of quantum mechanics, this goal became seemingly within the reach. With some standard approximations, such as the Born-Oppenheimer approximation, most of chemistry has been encoded in the simple mathematical form of the time-independent Schrödinger equation,

$$\hat{H}|\Psi\rangle = E|\Psi\rangle \tag{1.1}$$

where $\hat{H}$ is the Hamiltonian operator and $|\Psi\rangle$ an electronic wavefunction, an object that describes the behavior of electrons. The Hamiltonian operator looks innocent

(in this work, Einstein summation convention is mostly employed),

$$\hat{H} = H_0 + h_{\mu\nu}c_\mu^\dagger c_\nu + \frac{1}{2}V_{\mu\nu\lambda\sigma}c_\mu^\dagger c_\nu^\dagger c_\sigma c_\lambda. \tag{1.2}$$

Here, H_0 is a constant, like a nuclei repulsion energy, h is the one body operator describing the kinetic energy of electrons and their attraction to nuclei,

$$h_{\mu\nu} = \int d\vec{x}\, \mu^\star(\vec{x})(-\frac{1}{2}\nabla^2 - \sum_A \frac{Z_A}{\vec{r}_{1A}})\nu(\vec{x}), \tag{1.3}$$

with Z_A being the charge of nucleus A and $\vec{r}_{1A}$ the distance of an electron from that nucleus. The functions μ are the single particle orbits in which we express the Hamiltonian. The last term, V, represents the mutual electron repulsion

$$V_{\mu\nu\lambda\sigma} = \int d\vec{x}_2 \int d\vec{x}_1\, \mu^\star(\vec{x}_1)\nu^\star(\vec{x}_2)\frac{1}{r_{12}}\sigma(\vec{x}_2)\lambda(\vec{x}_1). \tag{1.4}$$

In the above, $\vec{x}$ represents the spin and spatial degrees of freedom. Finally, the operators $c_\mu^\dagger$ and c_μ create and annihilate a single particle state $|\mu\rangle = c_\mu^\dagger|-\rangle$ with $|-\rangle$ being the vacuum.

Even though the Hamiltonian admits such a simple form, the presence of the two body interaction (electron-electron interaction) means that the solutions to the Schrödinger equations for molecular systems remain elusive.

1.2 Two opposite ends: Hartree-Fock and exact diagonalization

As we outlined in the previous section, the Schrödinger equation describes the movement of electrons, which is the heart of chemistry. However, using quantum mechanics to perform chemical predictions requires solving for the many-body wavefunction; a computationally nontrivial task.

As the main point of this thesis is to introduce and benchmark approximate methods for solving the Schrödinger equation, let us begin by explaining how to obtain the exact wavefunction. At this point, let us note that by expressing the Hamiltonian in a finite basis of single particle states, an approximation has been already made. Fortunately, by extending the flexibility of said basis one may obtain a more and more accurate description of the wavefunction. Therefore, by "exact" we mean the eigenfunction of the Hamiltonian obtained within a given level of basis set truncation.

Let us imagine that one is interested in a particular system composed of N electrons. Moreover, there are M single particle states in the basis. We can therefore form any allowed N particle wavefunction by choosing N out of M creation operators and acting on the vacuum, denoted $|-\rangle$. In other words, we form sets $\{c^\dagger \ldots\}_i$ and create a state $|\Phi_i\rangle$ (so called Slater determinant) as

$$|\Phi_i\rangle = \{c^\dagger \ldots\}_i |-\rangle. \tag{1.5}$$

We express the Hamiltonian in the basis of said states $H_{ij} = \langle \Phi_i | \hat{H} | \Phi_j \rangle$ and diagonalize it. This allows us to represent a given eigenstate j of the Hamiltonian as

$$|\Psi_j\rangle = d_{ij} |\Phi_i\rangle, \tag{1.6}$$

with d_{ij} being the components of jth eigenvector of H.

This procedure to find a molecular wavefunction is not only exact but also conceptually simple. Unfortunately, as the reader may have noticed, in order to implement such an approach, one has to choose every possible combination of N objects out of the set of M states. Even a mediocre basis for the hydrogen atom contains 10 single particle states (spin-orbitals). Solving a very simple system of 10 interacting hydrogen atoms requires therefore diagonalizing a matrix of dimension $\approx 10^{13}$. Of course, using symmetry constrains, one can bring the dimension down. For example,

considering only $S_z = 0$ determinants one can reduce the dimension of the above problem by roughly a factor of 4. Nonetheless, the exact digitalization (also called Full Configuration Interaction -FCI) remains computationally intractable.

1.2.1 Hartree-Fock and the electron correlation

We hope that previous section convinced the reader that the exact solution of the many-body problem in quantum chemistry borders on being a trans-computational task. If choosing all possible Slater determinants is beyond reach, what would happen if one chooses only one? Clearly, an arbitrary choice of N creation operators (or choosing a set of N orbits) by no means guarantees any sensible answer. In order to hope for a reasonable description of the system one therefore performs a change of single particle basis

$$p^\dagger = \mathbb{D}_{\mu p} c_\mu^\dagger \tag{1.7}$$

and chooses typically the first N states $|p\rangle$ to create a Slater determinant $|0\rangle$. If the transformation $\mathbb{D}$ is chosen in a way that the energy of that determinant $\langle 0|\hat{H}|0\rangle$ is minimized one arrives at the celebrated Hartree-Fock (HF) theory . [6, 7]

In order not to digress too far from the main topic of this thesis, we do not include the derivation of the HF theory. Nonetheless we would like to point out that the HF determinant is an eigenstate of an effective one body operator $\hat{f}$, the Fock operator with matrix elements,

$$f_{pq} = h_{pq} + \sum_i \bar{V}_{piqi} \tag{1.8}$$

with $\bar{V}_{piqi} = V_{piqi} - V_{piiq}$ and the summation over i limited to the single particle orbits included in the state $|0\rangle$. The reader may notice that the two-body operator has been replaced by an effective one-body operator. The physical interpretation of this
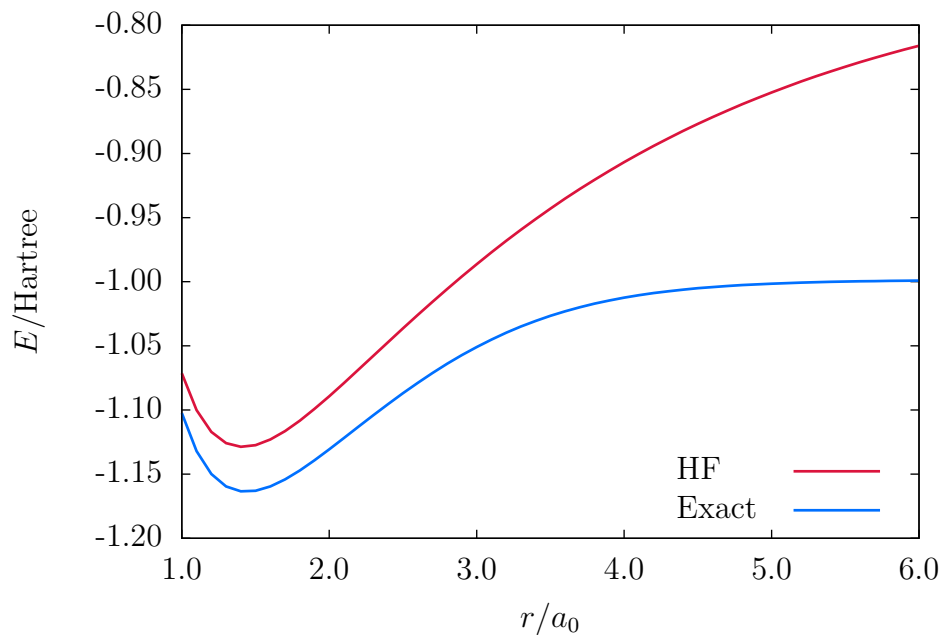
Figure 1.2.1 : Potential energy of H_2 molecule as a function of bond length. The data show exact (within the cc-pVDZ basis) and HF energies, a classical example defining weak and strong correlations. See text for details.

simplification is that the electrons cannot instantaneously react to the mutual change of their position. On the contrary, the electrons see only the average or the mean distribution of the other electrons. This means that their movement is uncorrelated, which is not correct since they repel each other via Coulombic interaction.

Here we arrive at the central object of the current thesis: electron correlation. Even though electron correlation is defined as just the difference between the exact energy and the energy of the Hartree-Fock determinant, this single number, in the author's opinion, is probably the most partitioned quantity in quantum chemistry. The literature is full of jargon about strong or static, dynamic or weak electron correlation, *etc.* To give the reader a feeling of what quantum chemists intuitively

mean by those types of correlation, let us consider the simple example of hydrogen molecule dissociation. The results of calculations with HF and the FCI are shown in Fig. 1.2.1. The HF reference is constrained to be an eigenstate of $\hat{S}^2$ operator. Usually, the correlation is measured with respect to HF determinant that obeys the spin symmetry. Clearly, close to the equilibrium bond length, the HF description of the system does not deviate significantly from the exact answer. To illustrate that point, let us consider that we only express the Hamiltonian in terms of the 1s orbitals of the atom on the left and the atom on the right, s_L and s_R, respectively. The optimal basis for the determinant is composed from the σ bonding and $\sigma^\star$ anti-bonding orbitals

$$|\sigma\rangle = \frac{1}{\sqrt{2}}(|s_L\rangle + |s_R\rangle) \tag{1.9}$$

$$|\sigma\rangle^\star = \frac{1}{\sqrt{2}}(|s_L\rangle - |s_R\rangle). \tag{1.10}$$

The RHF determinant is

$$|0\rangle = c_{\sigma,\alpha}^\dagger c_{\sigma,\beta}^\dagger |-\rangle. \tag{1.11}$$

Clearly, this state can be expressed in the terms of the underlying basis as

$$|0\rangle = \frac{1}{2}(c_{s_L,\alpha}^\dagger c_{s_L,\beta}^\dagger + c_{s_R,\alpha}^\dagger c_{s_R,\beta}^\dagger + c_{s_L,\alpha}^\dagger c_{s_R,\beta}^\dagger + c_{s_R,\alpha}^\dagger c_{s_L,\beta}^\dagger)|-\rangle. \tag{1.12}$$

In the above, the first two terms correspond to the configuration where both electrons are on the same atom, so called ionic states, whereas the last two represent the situation where each electron is on a separate nucleus. If we now ask what the probability of finding an electron with spin down on the left nucleus and an electron with spin up on the right nucleus is (with the operator $c_{s_L,\beta}^\dagger c_{s_L,\beta} c_{s_R,\alpha}^\dagger c_{s_R,\alpha}$) we will find that it is $\frac{1}{4}$. Similarly, the probability of finding an electron with spin up and

down on the same nucleus is also $\frac{1}{4}$. This is clearly incorrect since the electrons repel; the presence of one electron in the vicinity of a given nucleus should increase the probability of the second electron being on the other side of the molecule. Close to equilibrium, the qualitative agreement between FCI and HF suggests that such correlation between electrons in weak. However, as the bond distance increases, the ionic contributions must vanish. Indeed, the exact wavefunction should become $\frac{1}{\sqrt{2}}(c_{s_L,\alpha}^\dagger c_{s_R,\beta}^\dagger + c_{s_R,\alpha}^\dagger c_{s_L,\beta}^\dagger)|-\rangle$. Now, the expectation value of $c_{s_L,\beta}^\dagger c_{s_L,\beta} c_{s_R,\alpha}^\dagger c_{s_R,\alpha}$ is $\frac{1}{2}$, meaning that the electrons always stay at the opposite nuclei. In other words, electronic correlation is strong.

In the jargon, strong correlation is usually associated with degeneracies and spontaneous symmetry breaking by the Hartree-Fock procedure. One often thinks that whenever a single Slater determinant is not a good approximation to the ground state the system is strongly correlated.

1.3   Importance of electron correlation

In the previous section we outlined the idea of electron correlation by explicitly pointing out the independent movement electrons, a consequence of the Hartree-Fock approximation. Let us however elaborate on this topic by discussing the physical consequences of neglecting this effect.

If one is only interested in the ground state energies, for most of the typical problems in chemistry, HF accounts for about 99% of the total energy. [8] Nonetheless, chemistry depends on the changes in the energy and in this relative quantity the errors in the description of the electronic correlation have a significant contribution. For example, in the case of atoms, [9] the HF excitation energies may be wrong by more than 40%, and the correlation contributions to ionization potentials, though

smaller, are still not negligible. The situation looks even worse in the case of electron affinities, where HF may fail to predict stability of certain negative ions. On top of that, the transition probabilities between states are also rather poor. Finally, let us mention the polarizability of the atoms, which usually also displays large dependence on the inclusion of the correlation effects. [10]

Let us now outline some of the aspects of correlation in molecules. Quoting Ref. [11], though difficult to generalize, lack of correlation leads to too short bonds at equilibrium, incorrect bond angles and errors in the dipole moments. This is of course, provided that HF even qualitatively predicts molecules to exists, as the atomization energies are underestimated. Moving towards chemical reactions, lack of proper description of electron correlation leads to too high reaction barriers, which can be understood by HF problems with stretched bonds. Finally, vibrational frequencies are also usually too high. [12]

So far, we have only mentioned properties that suffer an error due to neglecting electronic correlation, yet we have already described a variety of properties of chemical interest. Let us now point out physical phenomena that are only due to the electron correlation; Hartree-Fock theory fails to predict pure dispersion interaction [13], correlation bound anions [14] and the like.

Finally, for extended materials the impact of electron correlation can be observed not only in a similar fashion as in molecules, *i.e.* the lattice parameters, bulk moduli and fundamental gap but also it can give rise to various intriguing properties. The strong Coulombic repulsion in confined orbitals of d- and f-electron materials makes the independent particle picture inapplicable. Strong interaction makes the various degrees of freedom exhibit rich and exotic behaviour, very sensitive to external parameters. To name a few, large resistivity changes, huge volume changes across phase

transition, heavy fermion behaviour and colossal magnetoresitance. [15, 16] Not to mention high temperature superconductors which are examples of strongly correlated materials of great importance and are subject of great theoretical interest.

1.4 Approximated methods for electronic correlation

Up to this point we hope to have convinced the reader of the importance of the proper description of electron correlation in chemistry. Since the Hartree-Fock theory, by very definition, does not contain electronic correlation, and the exact solutions, even in small bases, are beyond the reach of current computational resources, the main task of quantum chemists is to develop and benchmark approximate methods. Over many years of theoretical development supported by rapid increase in accessible computational power, much progress has been made.

Before we try to establish the current state of quantum chemical tools, let us comment on what we believe should be the guiding principle in method development. The discussion is based on Ref. [17]. In order for the approximation to be useful, a theorist should strive to provide tools that can be applicable to a large variety of problems, not only the problems that are inexpensive to calculate. In other words, the approximate methods should be applicable to systems chemists care about. If the goal of quantum chemistry is to provide theoretical guidance for experimental chemists, the methods should be implemented in an efficient and easy-to-use fashion. However, before deeming a method worth implementing and being made available, a theoretical tool must be throughly benchmarked against systems where accurate data are available. Such benchmark studies allow one to build confidence in the predictive power of the model such that a user of a given tool can understand the strengths and weaknesses of the model and interpret the results appropriately.

With the above in mind, let us discuss the basic approximations that are well established in the community. As we know, a single Slater determinant is not sufficient for accurate treatment of chemical problems whereas inclusion of all determinants is computationally prohibitive. The rather intuitive idea is therefore to include only selected terms in the wavefunction expansion. If one starts with the HF determinants and considers only those determinants that can be obtained by limited number of excitations from the ground state the approximation is known as truncated configuration interaction. Usually, one stops only at the level of single and double excitations. This method however suffers from certain limitations, most importantly, the quality of the results deteriorates with the system size.

The revolutionary idea of coupled cluster, [18–21] outlined in section 3.4 allowed for a better parametrization of the many-body Hilbert space in terms of excited determinants. This not only provided a more accurate description of the electronic correlation as compared to the truncated CI method but did so with comparable computational cost [22, 23]. The coupled cluster method quickly became the gold standard in quantum chemistry as it proved to have great accuracy for weakly correlated systems [24, 25]. Coupled cluster is not, however, an ultimate solution. The strong correlation involved in multiple bond breaking processes requires one to go to high excitation level, which quickly becomes prohibitively expensive even for moderately large molecules. [26, 27] Nonetheless, coupled cluster theory is a very good approximation that is easy to use; it requires no special theoretical background and can be used by experimental chemists to support their work.

On the side of strong electron correlation, the commonly employed tool is the complete-active space self consistent field method [28–30] which can be thought of as solving for the exact wavefunction in the space of chosen single particle orbitals.

This method however requires *a priori* choice of the single particle space and has rather large computational cost. Other methods with an efficient parametrization of the many-body Hilbert space are also available, such as the projected Hartree-Fock method which allows for accurate treatment of strong correlation without choosing an active space. [31–33] Unfortunately, the quality of description is bound to deteriorate with the increase of the molecular size.

Finally, let us mention the workhorse of the quantum chemistry community for the past few decades, the density functional theory (DFT). This approach in principle replaces the need of computing the wavefunction as it parametrizes the ground state energy only by the electron density. [34, 35] A computationally efficient and exact way of performing this parametrization is unfortunately unknown and a plethora of approximate schemes have been devised over the years. [36, 37] Perhaps the best way to justify DFT is its incredible success, resulting in a tremendous number of publications where DFT was the tool of choice. Nonetheless, it may be considered a non-systematically improvable approach.

We have striven to give the reader a feeling of what the current state of quantum chemistry toolbox is. The choice of the approximations discussed above is clearly arbitrary and by no means close to exhaustive. The message though is clear. After many years of effort, an accurate and computationally feasible treatment of electronic correlation remains elusive and there is definitely much place for improvement. Whether a new approach aims to provide answers of the quality comparable with existing methods but at lower computational cost, or allows to make more accurate predictions at the same computational cost, all new methods let us learn about strengths and weakness of certain approximations and will hopefully lead to better approximations.

1.5 Aim of the study

Quantum chemistry remains an open and highly dynamic field, where the need of more accurate approximations stimulates continuous improvement of existing methods and the introduction of new approaches to tackle electron correlation. In this work we strive to contribute to this collective effort especially for the systems that are sufficiently large to be intractable by well-established and accurate tools.

In chapter 2 we describe the recently developed density matrix embedding theory and benchmark it against the exactly solvable one-dimensional (1D) Hubbard model. As outlined in section 1.4, in order for an approximation to be useful, it has to be shown to perform well for test cases where accurate or exact data is available. While this approach by itself is not a many-body method used to solve the electronic Hamiltonian, but rather an approach to identify physically relevant degrees of freedom in the form of an effective Hamiltonian, the resulting equations are solved with exact diagonalization.

Having established the accuracy of the method for the model system, in chapter 3, we apply the approximation to chemically relevant problems. For those cases, even the dimensions of the simplified problem may be to large to be solved exactly. We therefore employ a coupled cluster approach.

Finally, in chapter 4, we introduce and investigate a simplified coupled cluster scheme, pair coupled cluster doubles, that may be employed as a way of solving the effective Hamiltonian for rather large sizes of the Hilbert space of the problem. As this approach is new, we proceed to first benchmark the approximation for molecular problems in order to gain insights of the accuracy one may expect, without introducing extra complication of the embedding procedure in DMET. This research lead us to further investigate the stability problem of the coupled cluster method. We

consequently suggest a coupled cluster methods that exhibit remarkable stability for strongly correlated systems, a feature that is desirable for the many-body approaches to be applicable for impurity Hamiltonians.

Chapter 2

Density Matrix Embedding Theory for Model Systems

In the following chapter we shall introduce the key method employed in the present work, the density matrix embedding theory. In particular, I will focus on the physical interpretation of the approximations used therein as well as formulate several variants of the theory which are benchmarked against exactly solvable model systems. The discussion presented in this chapter is based on our published work, see Ref. [1].

2.1 Density Matrix Embedding Theory

As outlined in the previous chapter, the major obstacle in the treatment of electron correlation in extended systems arises from the tremendous number of single particle degrees of freedom. Density matrix embedding Theory (DMET) was introduced by Knizia and Chan [38, 39] as a computationally efficient approach to truncate the electronic degrees of freedom into a small, locally important subset.

In order to highlight the basic ideas behind DMET, let us consider an exact ground state $|\Psi\rangle$ for the system under study. With that state at hand one can perform a Schmidt decomposition of this wavefunction [40]:

$$|\Psi\rangle = \sum_i \lambda_i |\alpha_i\rangle |\beta_i\rangle, \tag{2.1}$$

where states $|\alpha_i\rangle$ and $\beta_i\rangle$ can be chosen such that the former represent some spatially localized part of the system, the fragment. The latter must then be a complement

spanning the rest of the system excluded from the fragment, the bath. The summation limit in the above summation is then limited by the dimension of the smaller of those two subspaces. With such bases at hand, one may then formally project the physical Hamiltonian onto the fragment and bath, defining the so called impurity Hamiltonian,

$$\hat{H} \to \sum_{ijkl} |\alpha_i\rangle|\beta_j\rangle\langle\alpha_i|\langle\beta_j|\hat{H}|\alpha_k\rangle|\beta_l\rangle\langle\alpha_k|\langle\beta_l| := \hat{H}_{\text{imp}}. \tag{2.2}$$

The key point to notice is that the size of the basis of the impurity Hamiltonian, even though many-body in principle, can be chosen much smaller than the one of original problem, if expressed in a single particle basis. As discussed by Knizia [38], the impurity Hamiltonian shares the same ground state as the original problem, provided that the projection is performed with the exact wavefunction; henceforth, the expectation values of $\hat{H}$ could be obtained by studying the $\hat{H}_{\text{imp}}$.

Though formally interesting, the above prescription offers no computational advantage as it assumes *a priori* knowledge of the solution to the problem at hand. In order to form a computationally useful tool, DMET replaces the exact ground state by its mean-field picture, a Slater determinant. With this approximation, the Schmidt decomposition can be easily performed and the impurity Hamiltonian can be expressed in terms of a few, locally relevant, single particle states. The consequences of said approximation and physical interpretation of fragment and bath states are outlined in the following section.

2.2 Schmidt Decomposition of Slater Determinant

The DMET computational procedure starts by solving the physical Hamiltonian at the mean-field level, here the Hartree-Fock (HF). To remind the reader, this yields a Slater determinant $|\Phi\rangle = \Pi_i a_i^\dagger |-\rangle$, where $|-\rangle$ is physical vacuum and $a_i^\dagger$ creates a

hole (occupied) state $|i\rangle$. The HF quasiparticles are defined by the underlying HF transformation $\mathbb{D}$ from bare fermion operators [7],

$$a_p^\dagger = \mathbb{D}_{\mu p} c_\mu^\dagger. \tag{2.3}$$

The basis μ is accounts for spin and spatial degrees of freedom. Let us choose a suitable μ basis in which one can easily define a subset of states connected to the fragment (for example the on-site basis of lattice models or localized molecular orbitals) and introduce a projector onto fragment states $\hat{P}_F := \sum_{\mu_F} |\mu_F\rangle\langle\mu_F|$ and its complement $\hat{P}_B = \hat{I} - \hat{P}_F$ which projects onto the bath. Following Ref. [41], we construct an overlap matrix $\mathbb{M}$,

$$\mathbb{M}_{ij} = \langle\phi_j|\hat{P}_F|\phi_i\rangle \tag{2.4}$$

with indices i and j being hole indices. This hermitian matrix can be diagonalized by a unitary transformation $\mathbb{V}$, $\mathbb{V}^\dagger\mathbb{M}\mathbb{V} = d$ where the diagonal matrix d ($d_i \in [0,1]$) contains at most $\min(n_e, n_F)$ non-vanishing eigenvalues, where n_e is the number of electrons in the system and n_F is the number of single particle states associated with the fragment. Let us assume in what follows we assume that $n_F \ll n_e$ as we generally consider only a small part of the system as a fragment. Moreover, let us assume that there are always n_F eigenvalues different from 0 and 1. If this assumption fails, one has to take a special care in constructing the Schmidt basis. This assumption generally holds for the fragment sizes treated in the current chapter, therefore a problem of linear-dependencies of the fragment and batch states shall be addressed in the chapter 3. Each of the eigenvectors corresponding to a non-zero eigenvalue of $\mathbb{M}$ gives rise to a normalized fragment state,

$$|f_i\rangle = \sum_j \frac{\mathbb{V}_{ji}^\star}{\sqrt{d_i}} \hat{P}_F|\phi_j\rangle \tag{2.5}$$

and a corresponding bath state

$$|b_i\rangle = \sum_j \frac{\mathbb{V}_{ji}^\star}{\sqrt{1 - d_i}} \hat{P}_B |\phi_j\rangle. \tag{2.6}$$

The single particles states that correspond to vanishing eigenvalues shall be denoted as the inert core states. One may think about the inert core states as states with negligible coupling to the fragment states, at least in the mean-field picture. In Appendix 3.A we present an alternative way of understanding the Schmidt decomposition of a Slater determinant and show that the additional properties of the overlap matrix $\mathbb{M}$. At this point let us just stress that due to the bounds on the number of nontrivial eigenvalues of $\mathbb{M}$ the number of active single particle states (fragment and bath) is limited by the chosen size of the fragment, *i.e.*, if the physics of the system can be reliably described by forming the impurity Hamiltonian of small fragment size, the dimension of the single particle Hilbert space of extended system can be efficiently reduced and approached with highly accurate many-body techniques. In particular, in the present work we neglect the inert core state while projecting the Hamiltonian. Now, the fragment and bath states become simple single particle orbits. As it can be shown (see Appendix 3.A), the mean-field density matrix in the basis of fragment and bath states carries an integer number of electrons; the number of electrons is moreover equal to the number of fragment single particle states. Therefore, one may think about the bath as an effective reservoir of electrons for the fragment. In particular, the superposition of states with different number of electrons in the fragment (form zero to n_F), can be achieved by assigning to each fragment a bath state. One can then treat the fluctuating number of electrons in the fragment by means of Hilbert space calculation in the fragment-bath space. This situation is analogous to the example of hydrogen molecule described in section 1.2.1. Assuming that left hydrogen is chosen

as a fragment and the right hydrogen as a bath, the bath states are needed to describe configurations with no electrons in the vicinity of the fragment. Moreover, the extra electron carried by the bath is needed to describe two electrons in the fragment space.

2.2.1 DMET Impurity Hamiltonian

Due to the approximations made in formulating the DMET problem one neither guarantees the exactness of the approach nor that the impurity Hamiltonian will yield physically significant results if no constraints supplement the formulation of the theory. In order to alleviate the problem one introduces an effective one-body potential v to the physical Hamiltonian for which the Slater determinant is obtained,

$$\hat{H} = \sum_{\mu\nu} h_{\mu\nu} c_\mu^\dagger c_\nu + \frac{1}{2} \sum_{\mu\nu\lambda\sigma} V_{\mu\nu\lambda\sigma} c_\mu^\dagger c_\nu^\dagger c_\sigma c_\lambda + \sum_{\mu\nu} v_{\mu\nu} c_\mu^\dagger c_\nu. \tag{2.7}$$

This effective potential in the current work is constrained to act only within fragment. For the extended periodic systems studied here we chose the fragment to be always commensurate with primitive cell. Then, the effective potential can be replicated periodically over the lattice. Now, armed with the representation of the fragment and bath single particle states in terms of the bare fermion basis, one can construct the DMET impurity Hamiltonian,

$$\hat{H}_{\text{imp}} = \sum_{pq} \tilde{h}_{pq} e_p^\dagger e_q + \frac{1}{4} \sum_{pqrs} \tilde{V}_{pqrs} e_p^\dagger e_q^\dagger e_s e_r + \sum_{pq} \tilde{v}_{pq} b_p^\dagger b_q, \tag{2.8}$$

where e denotes both, the fragment (f) and bath (b) bases, the embedding basis. The $\tilde{t}$ and $\tilde{V}$ are the one- and antisymmetrized two-body matrix elements on the physical Hamiltonian in the embedding basis, respectively. The $\tilde{v}$ denotes the additional effective potential. The reader should notice that this potential does not act in the fragment subspace of the impurity Hamiltonian. Again, let us stress that replacing a

correlated wave-function by a Slater determinant allowed us to retain the simplicity of working with the single particle basis with significant reduction of the electronic degrees of freedom.

As the dimension of the embedding basis is relatively small, a powerful and accurate electronic structure tool can be now employed to solve it. The goal of the procedure if to find an effective potential v (hence also $\tilde{v}$) such that a suitable convergence criterion is satisfied. In the original formulation, [38] one obtains v by minimizing

$$|\gamma - \gamma_0| = |\langle\Psi_{\mathrm{imp}}|e^{\dagger}e|\Psi_{\mathrm{imp}}\rangle - \langle\Phi|e^{\dagger}e|\Phi\rangle|, \tag{2.9}$$

which is the difference between the mean-field and correlated one-particle density matrices over the embedding basis. Alternative choices of the convergence criterion are described in the following section.

At convergence, the energy density of the fragment is computed according to

$$\epsilon = \sum_{f \in F}\left[\sum_{j}\tilde{h}_{fj}\gamma_{jf} + \frac{1}{4}\sum_{jkl}\tilde{V}_{fjkl}\Gamma_{klfj}\right], \tag{2.10}$$

where $\Gamma_{ijkl} = \langle e_k^{\dagger}e_l^{\dagger}e_j e_i\rangle$ is correlated two-particle density matrix of the impurity Hamiltonian. The index f in the equation above is summed over the fragment states only whereas indices j, k and l run over the entire embedding space. It should be stressed that the formula above is not a true expectation value of the physical Hamiltonian, hence the DMET energy expression is not an upper bound of the true energy.

2.3 Computational Details

2.3.1 Convergence Criteria

In the original formulation of DMET [38], the objective function minimized by the effective potential was expressed according to Eq. 2.9. Despite the success of this approach, demonstrated by high quality numerical results, it introduces certain limitations. First of all, as demonstrated in Appendix 3.A, the mean-field density matrix in the embedding basis is idempotent. It is therefore not possible, in general, to find an optimal effective potential that could satisfy a perfect match between the correlated and the mean-field one-particle density matrix. A correlated impurity solver yields a density matrix that is not idempotent, except in the trivial case of non-interacting particles. Moreover, as the trace of the mean-field density matrix over the fragment subspace is guaranteed to return the number of electrons per fragment (see Appendix 3.A), an imperfect match may lead to solutions to the impurity Hamiltonian that do not strictly represent the physical system one wishes to study. This is especially important for periodic, extended systems where the average number of electrons per fragment must be a well defined quantity. Moreover, as the energy density of a system is computed with the impurity Hamiltonian wavefunction, any error in the averaged density in the fragment affects the predictions for the entire system. For this reasons, in the current chapter, we shall define the objective function minimized by the effective potential as

$$\min_v \sum_{ff'} |\gamma - \gamma_0|_{ff'}. \tag{2.11}$$

Provided that a perfect match is found, as it was the case in the present study, this convergence criterion allows one to control the average filling of the fragment.

Following similar logic, one may further simplify the computations by requiring

only the diagonal elements of said density matrices to coincide. At this point, let us however note that due to the lack of invariance of the diagonal elements of the one-particle density matrix with respect to unitary rotations, by "diagonal" entries we understand the representation in the bare fermion basis, not the embedding basis. This is allowed as the fragment states of the embedding basis are related to the bare fermion basis by a unitary transformation. In this approach, referred to as density embedding theory (DET), one simply requires that the local density of the system is equivalent in the correlated impurity wavefunction and the mean-field solution used to construct the impurity problem. Such a decrease in the number of constraints is reflected in the simplification of the effective potential added to the physical Hamiltonian, *i.e.* Eq. 2.7 becomes:

$$\hat{H} = \sum_{\mu\nu} h_{\mu\nu} c_\mu^\dagger c_\nu + \frac{1}{2} \sum_{\mu\nu\lambda\sigma} V_{\mu\nu\lambda\sigma} c_\mu^\dagger c_\nu^\dagger c_\sigma c_\lambda + \sum_\mu v_{\mu\mu} c_\mu^\dagger c_\mu. \tag{2.12}$$

The numerical data and our experience suggest that the above approximation allows one to greatly facilitate the convergence properties of the approach while delivering results of similar quality to DMET.

2.3.2 Choice of mean-field

The original formulation of DMET for model systems neglected the effect of the two-body interaction in the Hamiltonian used to obtain mean-field solution as well as in the bath-bath block of the impurity Hamiltonian. [38] In this case, the entire system is approximated by a set of fully noninteracting particles and the Hartree-Fock determinant is the true ground state of the system. Due to this fact, no symmetry breaking in the mean-field may occur, unless, of course, the ground state is degenerate. We do not, however, consider here an explicitly symmetry-violating effective potential

which indeed may violate translational invariance whenever chosen fragment does not correspond to single primitive cell. We note that one may implicitly breaks other symmetries by allowing the effective potential to do so.

In the present work we explore a different procedure. The full system is described by the physical Hamiltonian, supplemented only by the effective potential. The Hartree-Fock transformation is not constrained to be an eigenfunction of the $\hat{S}^2$ operator but just the $\hat{S}_z$ operator. As a consequence, the impurity Hamiltonian does not need to commute with the $\hat{S}^2$ operator. However, in order to retain the simplicity of the spin-restricted formalism, the effective potential is diagonal in the spin space. Therefore, in order to determine its value, the spin diagonal block of the one-particle density matrix derived from HF and correlated wavefunction is used in the fitting procedure. This obviously does not affect the condition that a perfect match between this objects guarantees no violation of the average number of electrons per fragment. Moreover, let us stress that we do not attempt to fit the density matrix over the entire embedding basis as the spin-dependent bath states are not easily expressible in a common basis. The fragment states are related to bare fermion states by an invertible transformation but the bath states are not.

Finally, let us point out that the spin unrestricted formalism may lead to solutions for the full system that are not commensurate with the fragment size. In other words, charge fluctuations may be beyond the size of the fragment. In order to retain the simplicity arising from the periodicity of the extended systems we constrain the mean-field transformation to be periodic with a primitive unit cell of the size of the fragment. This can be easily done with the help of a translational symmetry-adapted bare fermion basis.

2.3.3 Impurity Solver

In the present chapter, the impurity Hamiltonian was solved by means of exact dig-italization. The Slater determinant basis has been constructed without employing $\hat{S}^2$ nor spatial symmetry. We have only enforced that $\langle S_z \rangle = 0$ and that the single particle basis is real.

2.4 Benchmark Calculations in the one-dimensional Hubbard Model

In the present section, we present benchmark calculations for the 1D Hubbard model,

$$\hat{H} = -t \sum_{\langle \mu\nu \rangle \sigma} c_{\mu\sigma}^{\dagger} c_{\nu\sigma} + U \sum_{\mu} c_{\mu\alpha}^{\dagger} c_{\mu\beta}^{\dagger} c_{\mu\beta} c_{\mu\alpha} \tag{2.13}$$

where $\langle \ldots \rangle$ denotes summation over nearest neighbours. This lattice Hamiltonian was chosen due to availability of exact solution *via* the Bethe ansatz (BA) solved by Lieb-Wu equations. [42–45] The results denoted as DMET(n) correspond to a spin-symmetry broken mean-field solution with convergence criterion defined by Eq. 2.11 and the fragment composed of n sites whereas DET(n) corresponds to the fit per-formed over the diagonal entries in the one-particle density matrix. For completeness, we include the results obtained with the original formulation of DMET of Ref. [38] where the two-body interaction is not present in the full lattice Hamiltonian nor in the bath block of the impurity Hamiltonian. We label those calculations as nonin-teracting, NI and NI$_F$ case. The additional subscript F "Full matrix" denotes that the fit of the density matrix is performed over the entire embedding basis (see Eq. 2.9). The calculations for NI$_F$ were performed with the program made available in Ref. [38].

2.4.1   Half-lattice embedding

Here we shall focus on a particular benchmark case where the chosen fragment spans half of the entire system. As outlined in Appendix 3.A, in such a case the total number of fragment and bath states has the same dimension as the bare fermion basis of the full problem. In other words, no core states are present in the Schmidt decomposition. As a consequence, no computational saving arises due to the embedding procedure. The results are shown in Table 2.1. Clearly, the DMET embedding scheme is not exact in this case. Due to the fact that the impurity Hamiltonian is the physical Hamiltonian for $v = 0$, but the mean-field density matrix does not agree with the exact one, the DMET equations require solution with non-vanishing effective potential. This leads to small but not negligible deviations of DMET from BA. On the other hand, the mean-field solution does not break translational symmetry of the charge density for systems studied; the DET convergence criterion is therefore satisfied by $v = 0$ and the impurity Hamiltonian and its solution corresponds to the physical Hamiltonian of the full lattice.

2.4.2   Half-filled Hubbard rings

Let us turn our attention to cases where embedding does offer significant computational savings. In the present work we choose a Hubbard ring of 400 sites where exact diagonalization becomes unfeasible. The energy density obtained with the embedding fragment size of 2 and 4 sites is presented in Fig. 2.4.1. As the reader may notice, even with the small fragment size, the DMET and DET predictions overlap well with the exact answer. The biggest error is observed for the intermediate coupling strengths. For the weak and strong coupling regimes the embedding provides accurate energies of the Hubbard model. One should also notice that DET agrees well

Table 2.1 : Energies per site (in units of t) for small Hubbard rings evaluated with D(M)ET approximations and Bethe Ansatz.

	8 sites U=				
	2	4	6	8	10
BA	-0.8210	-0.5754	-0.4261	-0.3333	-0.2721
DMET(4)	-0.8382	-0.5609	-0.4118	-0.3210	-0.2616
DET(4)	-0.8210	-0.5754	-0.4261	-0.3333	-0.2721
	4 sites U=				
	2	4	6	8	10
BA	-0.7071	-0.5257	-0.4087	-0.3301	-0.2750
DMET(2)	-0.7262	-0.5090	-0.3860	-0.3091	-0.2568
DET(2)	-0.7071	-0.5257	-0.4087	-0.3301	-0.2750

with DMET even though the errors are somehow larger. This supports our current choice of determining optimal fit between correlated and mean-field density matrices. By comparing to the embedding schemes introduces by Knizia and Chan [38] we observe improved quality of the description of the system introduced by spin symmetry breaking. We should also stress that performing a fit to the entire density matrix in the NI_F scheme is superior to fitting in the fragment space only. Nonetheless, every embedding approach presented in Fig. 2.4.1 for the fragment of 2 sites perform extremely well taking into account that the many-body Hilbert space of the problem was truncated from approximately 10^{238} to just 36 states.

Increasing the size of the embedded fragment to 4 sites, we notice systematic improvement of all presented approaches. DMET and DET based on spin symmetry

broken references are virtually indistinguishable from the exact answer. The NI$_\text{F}$ approach becomes noticeably more accurate as the fragment size increases. Only the NI approach shows significant deviations from the exact results at large coupling strength, yielding energies comparable to the symmetry broken Hartree-Fock approach, especially for U $\geq 8t$. Again, one should keep in mind that the dimension of the many-body Hilbert space used in these calculations was only 4900.

The accurate description of the energy density does not allow us to fully gauge the quality of the impurity wavefunction. We now turn our attention to a two-body correlation function, the double occupancy $\langle n_\downarrow n_\uparrow \rangle$. Correct description of this correlation function confirms that not only the total energy but also the individual components are reproduced well by the impurity Hamiltonian. Said correlation function was computed as $\frac{\langle \hat{U} \rangle}{U n_F}$ for the embedding schemes where $\hat{U}$ is the two body interaction operator in the fragment (we use the locality of the Hubbard interaction) and n_F is the fragment size. For the Bethe ansatz, the Hellmann-Feynman theorem was used, $\langle n_\downarrow n_\uparrow \rangle = \frac{\partial e}{\partial U}$. The results are shown in Fig. 2.4.2. Again, the spin symmetry broken formalism yields accurate results even with the smallest fragment size considered. On the scale of the plot, the data is almost indistinguishable from exact values. The embedding schemes arising from a noninteracting lattice deviate more significantly from the BA, especially at larger values of interaction strength. This is consistent with the behaviour of the energy density. Increasing the fragment size improves the already good predictions of symmetry broken DMET and DET. The improvement of NI$_\text{F}$ is more significant. The discrepancy with BA can be now only observed for intermediate coupling strength. Consistently with the energy density, NI offers the worst predictions of the double occupancy of all the methods studied here.
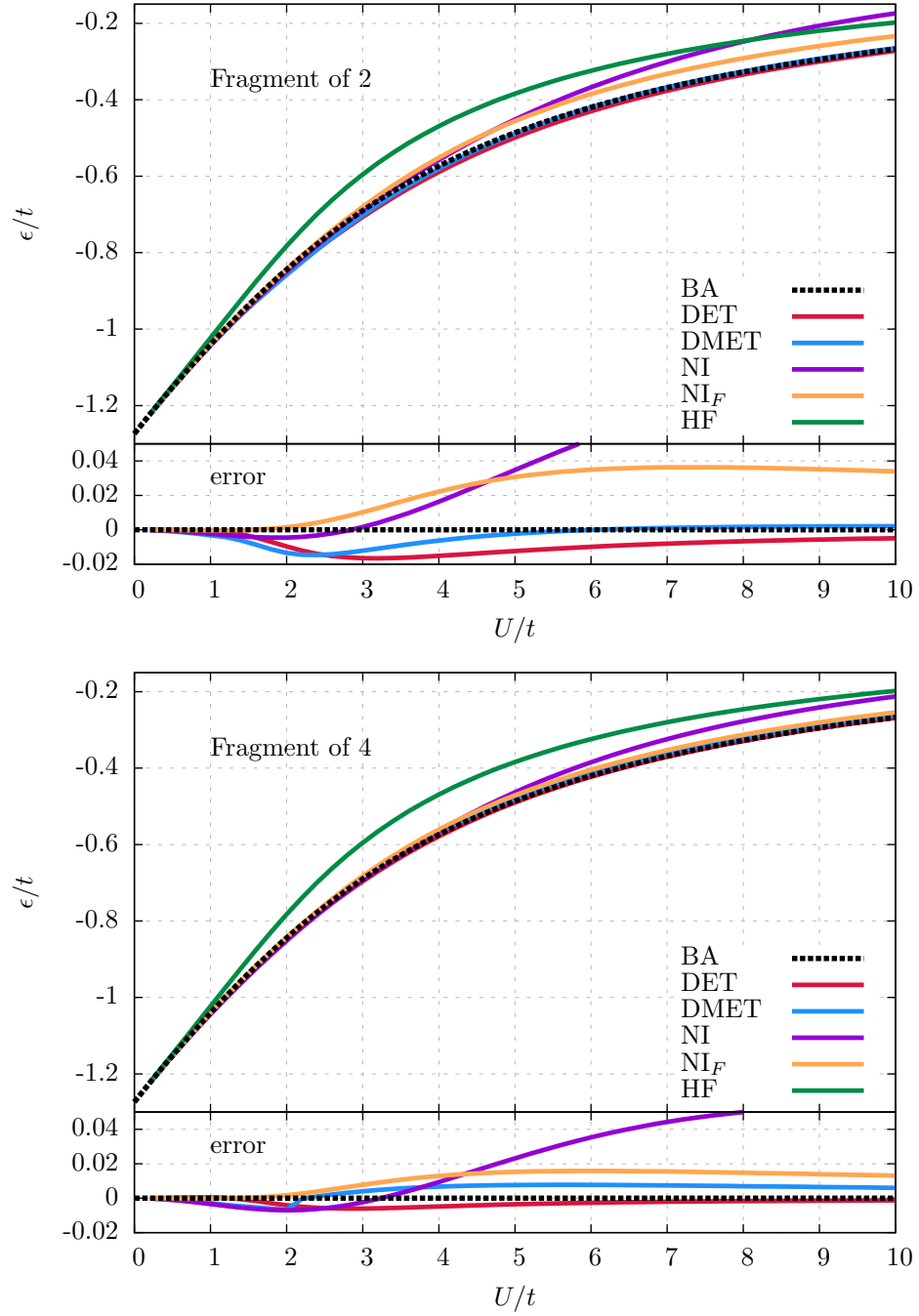
Figure 2.4.1 : Energy per site of the 1D Hubbard model at half-filling evaluated with various embedding schemes with a fragment of 2 (top panel) and 4 sites (bottom panel). Bethe ansatz (BA) results are added for comparison. Figure taken from Ref. [1].
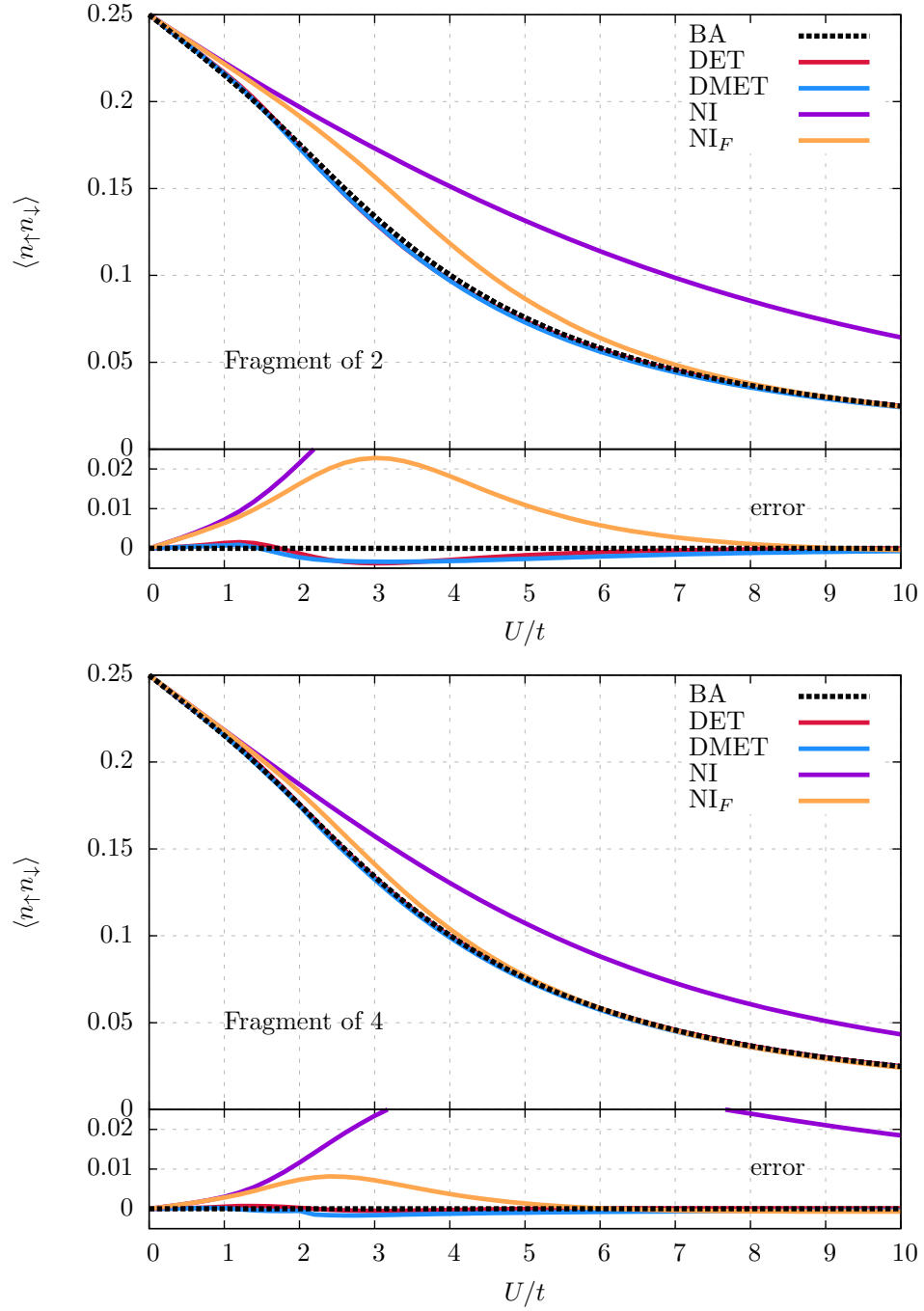
Figure 2.4.2 : Comparison of double occupancy for the 1D Hubbard model at half-filling evaluated with various embedding schemes with fragment of 2 (top) and 4 sites (bottom). The Bethe ansatz (BA) results are added for comparison. The error with respect to BA is plotted in the bottom panel. Figure taken from Ref. [1].

2.4.3   Hole-dopped Hubbard rings

As demonstrated in the preceding section, the broken symmetry DMET and DET offer good description of the half-filled Hubbard model at any value of the interaction strength. Let us now turn our attention to another parameter defining the model, the filling fraction. In Fig. 2.4.3 and Fig. 2.4.4 we present the energy density as a function of filling fraction $\langle n \rangle$ for the 400 sites Hubbard ring at $U = 4t$, $6t$ and $8t$. Additionally, we plot the percent error with respect to the exact answer.

As the reader may readily notice, for the lower interaction strengths presented, all of the embedding schemes offer reasonable description of the model. We do not observe errors beyond 4% at any filling fraction. For the fragment of 2 sites and $U = 4t$, we observe a good agreement between DMET and DET until around filling fractions of 0.75, where broken-symmetry DMET starts deviating from the BA noticeably more than DET. We also observe that the NI_F approach seems to be slightly better than the embedding schemes introduced in the present work. Let us stress however that we were able to find a global minimum of the minimized objective function of all of the systems, hence no error in the particle number was present. As the function $\epsilon(\langle n \rangle)$ shows not a negligible slope, any changes in the average particle number can affect the results. In the case of $U = 4t$, we also present the curve for fragment of 4 sites evaluated with DET. One can observe a noticeable improvement with respect to DET(2) calculations and small error in the entire range of filling fractions studied.

For the larger values of U, we can see that DMET and DET based on spin symmetry broken mean-field solutions becomes more accurate than the original NI_F formulation for most of the studied filling fraction. Only for very heavily doped systems does the description provided by those approaches become similar. The reader should notice that the difference of convergence schemes employed does not lead to notice-
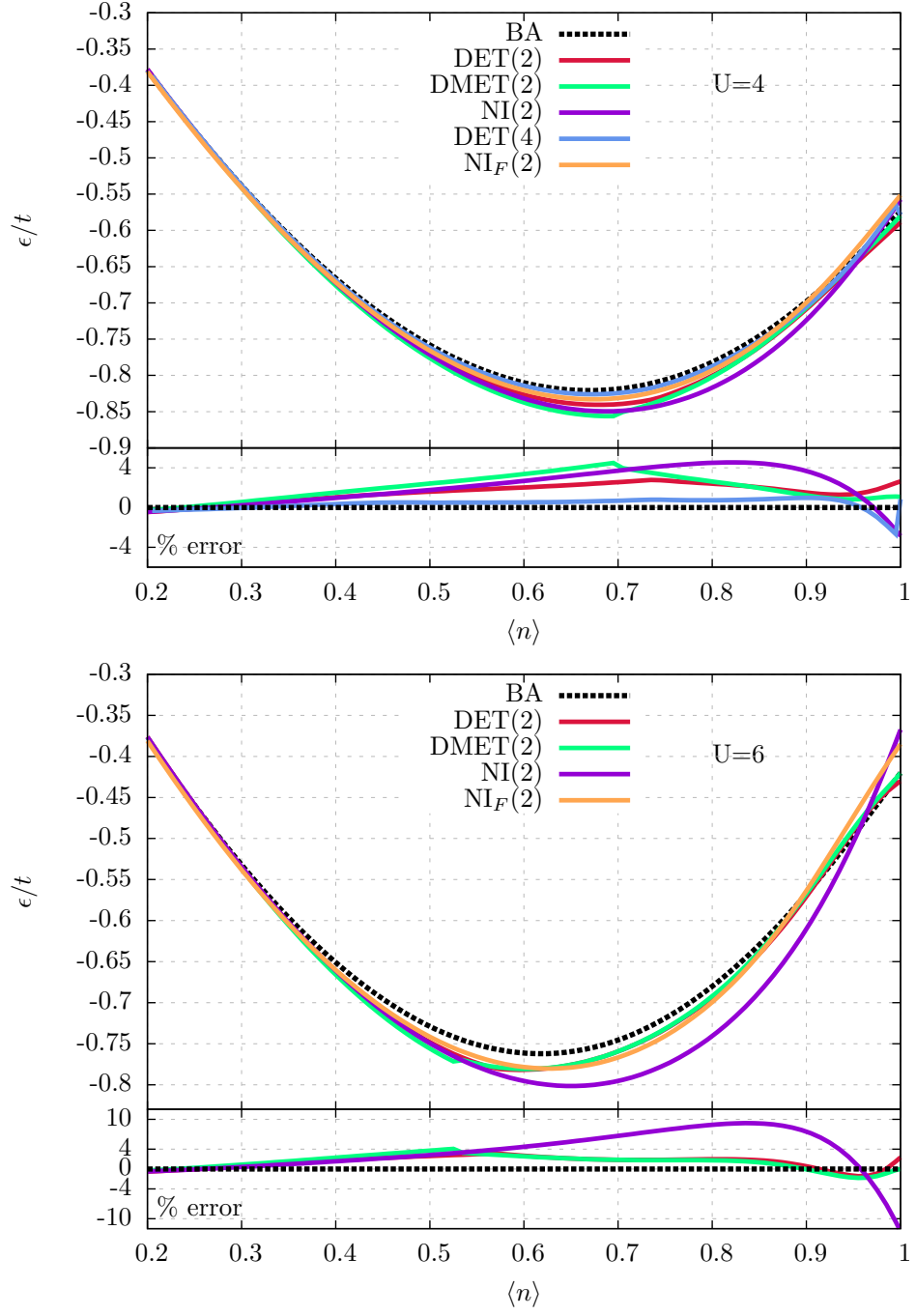
Figure 2.4.3 : Energy density of the 1D Hubbard model as a function of the filling fraction evaluated with various embedding schemes for U = 4t (top) and U = 6t (bottom). Bethe ansatz results are added for comparison. The percent error with respect to BA are plotted in the bottom inset. Figure taken from Ref. [1].
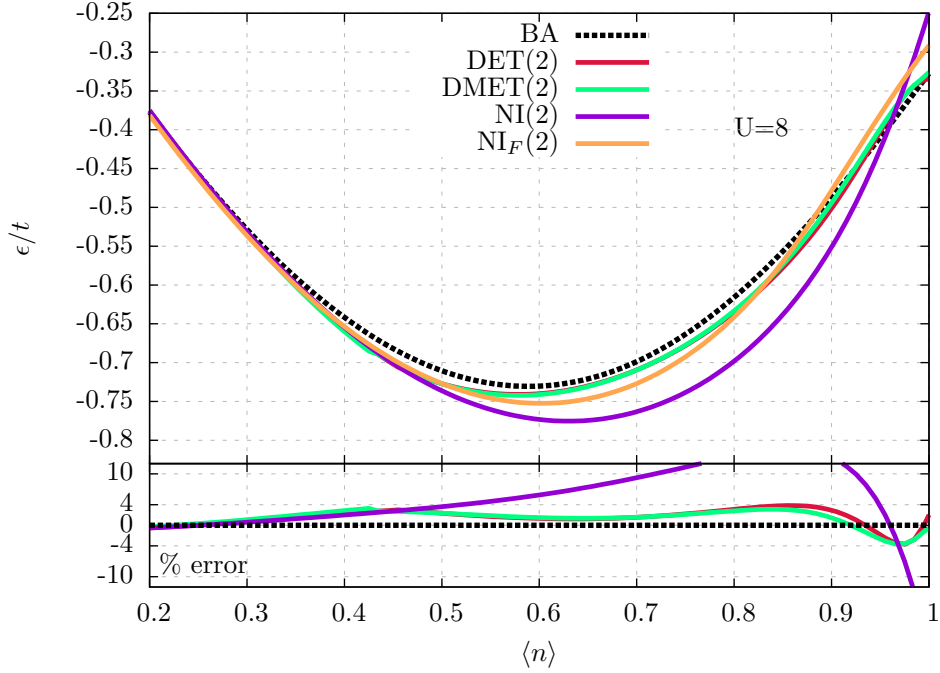
Figure 2.4.4 : Energy density of the 1D Hubbard model as a function of the filling fraction evaluated with various embedding schemes for U = 8t. Bethe ansatz results are added for comparison. The percent error with respect to BA are plotted in the bottom inset. Figure taken from Ref. [1].

able differences in results as DMET and DET curves overlap very well. Interestingly, the error again does not exceed the 4% level. Analogous to the half-filled case, we observe that enforcing a perfect match between the mean-field and correlated density matrices over the fragment space (NI approach) leads to significant deviations from the BA for large values of U. The NI scheme clearly leads to the poorest description of the energetics of the system for most doping regimes.

Finally, let us point out that after a certain doping fraction, the mean-field solutions we were able to find cease to spontaneously break spin symmetry. This leads to small, but unpleasant kinks in the DMET and DET curves.

Let us now proceed to benchmark spin-symmetry broken embedding for doped systems in more detail. To do so, we study the lattice density as a function of chemical potential. The data in the current work was obtained by minimizing

$$\hat{H}_\mu = \hat{H} - \mu\hat{N} \tag{2.14}$$

with respect to electron number at given chemical potential μ. Here $\hat{H}$ is the Hubbard Hamiltonian and $\hat{N}$ is the number operator. We compare the symmetry-broken mean-field embedding to the NI scheme only. The analogous data for NI_F can be found in the literature, see Ref. [38]. The behaviour of the average density as a function of chemical potential was used by ground state techniques to gauge metal-insulator transitions. [38, 46] Vanishing derivative of density with respect to chemical potential is identified with the incompressible insulating state.

The results for the fragment size of 2 are presented in Fig. 2.4.5. It is clear that the NI approach clearly does not reproduce any transition, even qualitatively; NI_F was reported to provide quantitatively correct behaviour. We conclude therefore that employing a noninteracting reference for embedding calculations suffers from restraining the correlated density matrix to exactly match the mean-field one over the fragment space. In the DET approach the transition is clearly visible and quantitatively correct. The reader may notice that an abrupt jump in the $\langle n \rangle(\mu)$ curve which implies that certain filling fractions are not stable at any chemical potential. This error can be traced back to the behavior of the energy density versus filling fraction. As is clear from Fig. 2.4.3 and Fig. 2.4.4, the DET approach yields a little too low energies for the half-filled lattice and significantly doped lattices and larger energies at very small doping fractions, as compared to BA. This implies that the small doping fractions are fictitiously under-stabilized in the current approach. Again, one may also notice some discontinuities at small filling fractions arising from the transition of spin symmetry
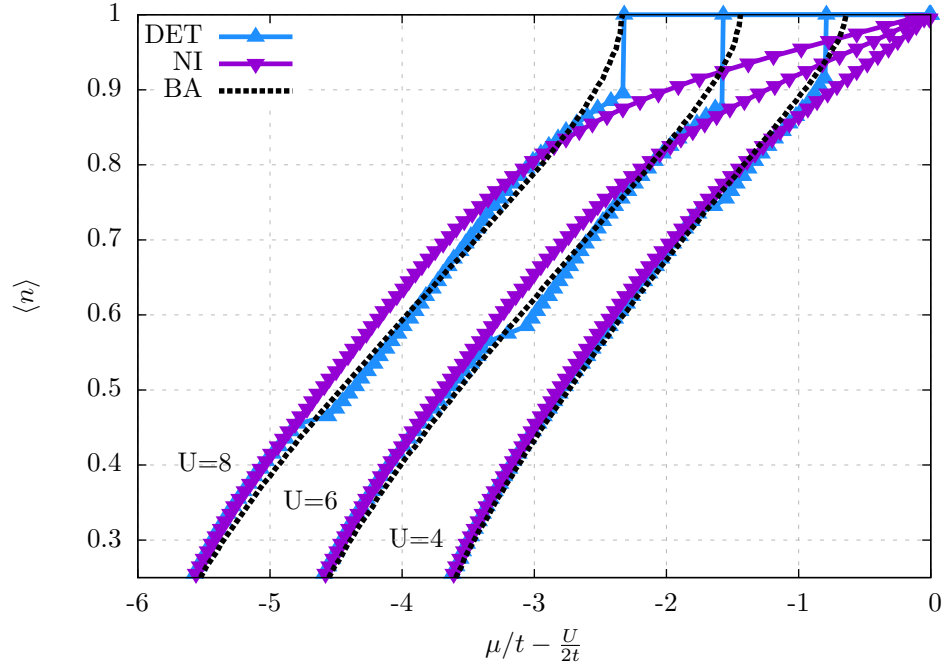
Figure 2.4.5 : Lattice filling as a function of chemical potential evaluated with various embedding schemes and the fragment size of 2 lattice sites. Exact Bethe ansatz data is shown for comparison. Figure taken from Ref. [1].

broken to spin preserving solutions. Despite these formally unpleasing features, the DET results predict the transition at chemical potentials close to the exact ones. The impact of the fragment size used for embedding is presented in Fig. 2.4.6. The reader may verify that for $U = 4t$ the fragment of 4 sites offers significant improvement over fragment of 2, not only for the point of chemical potential at which the transition occurs but also in the size of the unstable filling fractions. The NI approach does not yield any sort of transition even with the larger fragment.
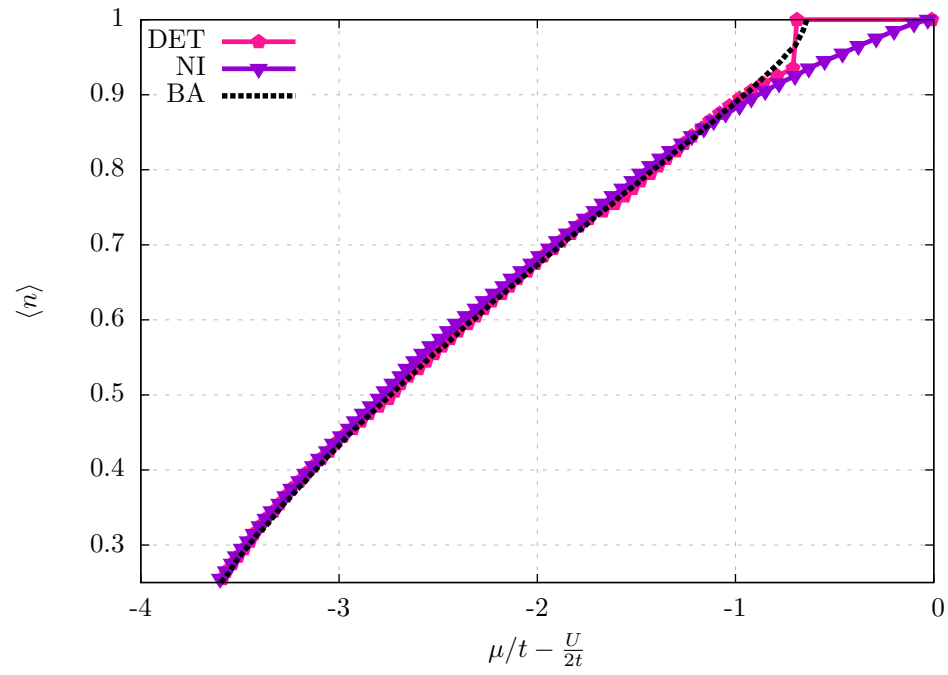
Figure 2.4.6 : Lattice filling as a function of chemical potential evaluated with various embedding schemes and the fragment size of 4 lattice sites. Exact Bethe ansatz data is shown for comparison. Figure taken from Ref. [1].

2.4.4   Long-range properties

So far we demonstrated that density matrix embedding theory can be considered a fairly accurate approach for the description of the energetics of the Hubbard model as well as its local properties. In this section, we wish to remind the reader that the intrinsically local picture included in the approximation may fail. To this end, we study the spin-spin correlation function (SSCF),

$$\text{SSCF}(j) = \langle \hat{S}_1 \cdot \hat{S}_j \rangle,$$

where $\hat{S}_j$ is the spin operator at site j. In order to evaluate this property, we transform the on-site representation of said operator into the embedding basis and evaluate it with the exact solution for the impurity problem. At this point we note that alternatively one may evaluate this operator with the inclusion of the core states neglected in the impurity Hamiltonian. However, as the core state are neglected in the evaluation of the energy and we want to study the long-range properties included in the embedding basis, we do not attempt to do it here. Therefore, the discussion here presents the extent at which the bath states spread into the full lattice and are aware of the distant parts of the system. Finally, let us stress that the site 1 has been chosen as the first site of the embedded cluster.

In Fig. 2.4.7, we present the SSCF for the 8-sites Hubbard ring at half-filling with the fragment of 4. Once again, this corresponds to the case where the embedding scheme offers no computational advantage. The spin-symmetry broken DET approach constitutes here the exact solution so the SSCF overlaps perfectly with the exact data. The DMET self-consistency criteria are not however satisfied by vanishing effective potential and the solution deviates for the exact ground state. This affects the SSCF which deviates somewhat from the exact correlation function. Proceeding to larger

lattices, here 30 sites with 30, 26 and 22 electrons (Fig.2.4.8), we observe that the DET approach deviates significantly for the exact data for virtually all site indices not included in the fragment. In order to illustrate it in more detail, Fig. 2.4.8 contains also single particle basis coverage defined as

$$\frac{1}{2} \sum_e \langle e | \hat{P}_j | e \rangle \tag{2.15}$$

where the summation runs over the embedding basis and $\hat{P}_j$ is the projector on site j. Clearly, the sites included in the fragment are fully represented by the embedding single particle states in the impurity Hamiltonian. The contributions to the bath states, however, decay rapidly with the distance from the fragment, especially at half-filling. This effectively screens the long-range information resulting in rapid decay of the SSCF.

2.5   Conclusions

In the present chapter, we have investigated several possible DMET schemes within the spin-symmetry broken formalism. We included the effects of the two-body interaction in the lattice mean-field. We have shown that fitting the diagonal of the fragment density matrix leads to results of similar quality to the full method while our experience shows that the convergence of the method is significantly improved. The numerical data suggests that the current approach yields very good description of the energetics and the local properties of 1D Hubbard model. For the hole-doped systems, the approach predicts good Mott gaps and density profiles.

As formulated, the current approach does not provide a good description of the correlation functions beyond the size of the fragment. From this perspective, developing and benchmarking reliable and accurate impurity solvers that allow for the
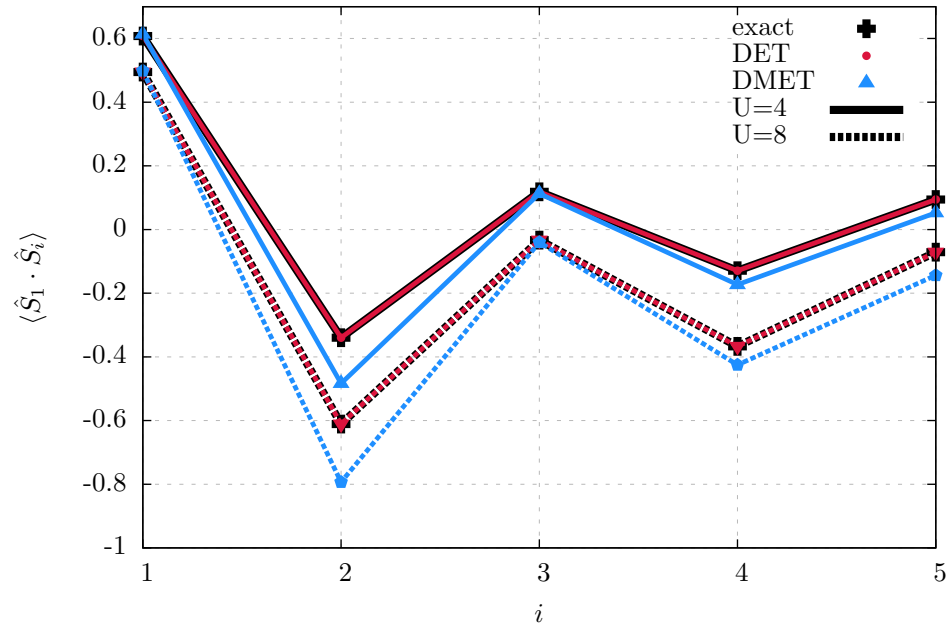
Figure 2.4.7 : Spin-spin correlation function for 8 sites Hubbard ring at half-filling evaluated with DMET and DET. The embedded fragment size is composed of 4 sites. For clarity, the results for U=8t are shifted down by 0.2. Figure taken from Ref. [1].
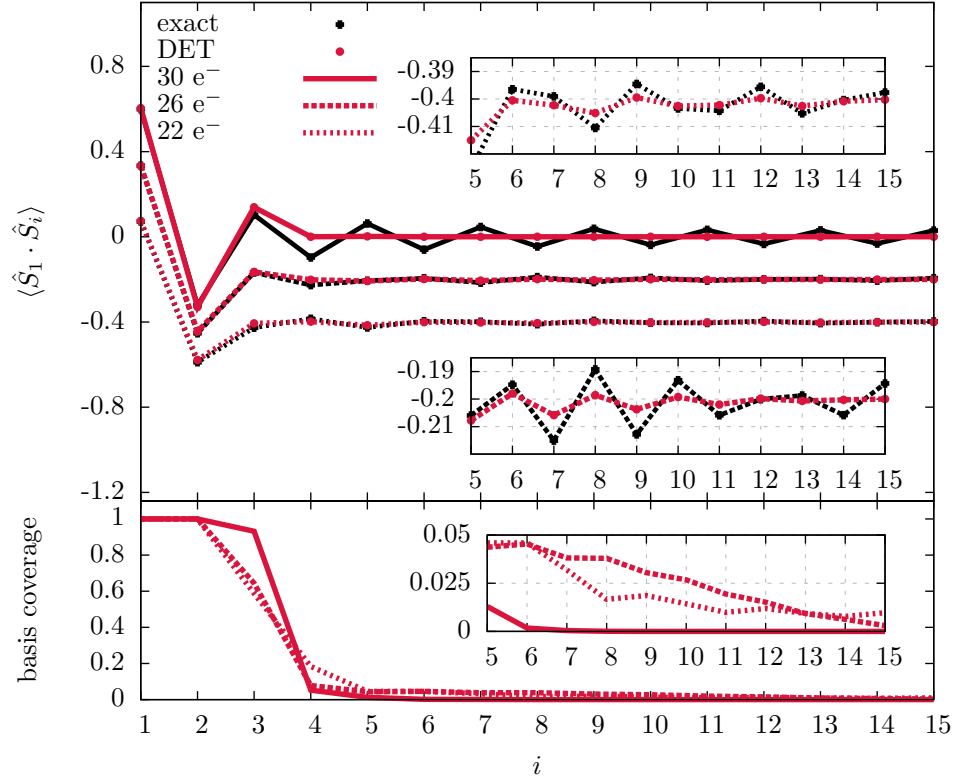
Figure 2.4.8 : DET spin-spin correlation functions evaluated for a ring of 30 sites with 30, 26 and 22 electrons at U=4t. For clarity, data for 26 and 22 electrons are shifted down by 0.2 and 0.4, respectively. The bottom panel represents the basis set coverage (see text for details). Figure taken from Ref. [1].

treatment of larger fragment sizes is important and it will be discussed in chapter 4.

Appendix

2.A   Schmidt Decomposition of Salater Determinant

In the following, we shall investigate some properties of the embedding basis. In particular, we show that the mean-field density matrix in embedding basis must be idempotent and commute with the mean-field Fock matrix in the embedding basis.

2.A.1   Complete set of states

In the following, we will use indices i, j, k and l for the hole states and a, b, c and d for particles states. Let us define matrices

$$\mathbb{M}_{ij} = \langle j|\hat{P}_F|i\rangle \tag{2.16}$$

$$\mathbb{M}_{ab} = \langle b|\hat{P}_F|a\rangle \tag{2.17}$$

$$\mathbb{M}_{ia} = \langle a|\hat{P}_F|i\rangle. \tag{2.18}$$

Clearly, the matrices $\mathbb{M}_{ij}$ and $\mathbb{M}_{ab}$ can be diagonalized by a unitary transformation $\mathbb{V}$ and $\mathbb{U}$, respectively. Their eigenvalues d are bound in $[0, 1]$.

Let us assume that the number of single particle fragment states is bigger neither than the number of particles nor holes in the system. Moreover, let us assume that all eigenvalues of the matrices $\mathbb{M}_{ij}$ and $\mathbb{M}_{ab}$ that could possibly be different from 0 or 1, actually *are* different from 0 or 1. Otherwise, linear dependencies exist. We shall deal with such situation in the next chapter.

From the matrices $\mathbb{M}_{ij}$ and $\mathbb{M}_{ab}$ one can form n_f orthonormal fragment and bath

states and $n_h - 2n_f$ and $n_p - 2n_f$ core states where n_h (n_p) is the total number of holes (particles). We shall now prove that the fragment and bath states obtained from $\mathbb{M}_{ij}$ and $\mathbb{M}_{ab}$ span the same space, to which the core states are orthogonal. In other words, we show that the fragment states obtained from hole orbitals

$$|f_i\rangle = \frac{\mathbb{V}_{ki}^\star \hat{P}_F |k\rangle}{\sqrt{d_i}} \tag{2.19}$$

and the particle states

$$|f_a\rangle = \frac{\mathbb{U}_{ba}^\star \hat{P}_F |b\rangle}{\sqrt{d_a}} \tag{2.20}$$

are the same up to a phase, just as their corresponding bath states,

$$|b_i\rangle = \frac{\mathbb{V}_{ki}^\star \hat{P}_B |k\rangle}{\sqrt{1 - d_i}} \tag{2.21}$$

and the particle states

$$|b_a\rangle = \frac{\mathbb{U}_{ba}^\star \hat{P}_B |b\rangle}{\sqrt{1 - d_a}}. \tag{2.22}$$

However, the core states (corresponding to vanishing eigenvalues) obtained from the hole basis,

$$|c_i\rangle = \mathbb{V}_{ki}^\star \hat{P}_B |k\rangle \tag{2.23}$$

and particle basis

$$|c_a\rangle = \mathbb{U}_{ba}^\star \hat{P}_B |b\rangle \tag{2.24}$$

are orthogonal to each other and to fragment and bath states.

Lemma 1. *A column vector $\mathbb{U}_{ba}$ which is an eigenvector of $\mathbb{M}_{ab}$ corresponding to eigenvalue d_a satisfies the following relation,*

$$\mathbb{M}_{ck} \mathbb{M}_{kb} \mathbb{U}_{ba} = (d_a - d_a^2) \mathbb{U}_{ca}. \tag{2.25}$$

Proof. Using resolution of identity and the fact that the projector operator is idempotent we quickly get,

$$\mathbb{M}_{cb}\mathbb{U}_{ba} = \mathbb{M}_{ck}\mathbb{M}_{kb}\mathbb{U}_{ba} + d_a^2\mathbb{U}_{ca} = d_a\mathbb{U}_{ca}, \tag{2.26}$$

hence

$$\left[\mathbb{M}_{ck}\mathbb{M}_{kb}\right]\mathbb{U}_{ba} = (d_a - d_a^2)\mathbb{U}_{ca}. \tag{2.27}$$

$\square$

Lemma 2. *A vector $\mathbb{M}_{ib}\mathbb{U}_{ba}$ is a null vector whenever vector $\mathbb{U}_{ba}$ is an eigenvector of $\mathbb{M}_{ab}$ with eigenvalue 0 or 1 and it is not a null vector otherwise.*

Proof. Let us define n_p column vectors $\mathbb{X}_{ia} = \mathbb{M}_{ib}\mathbb{U}_{ba}$. The overlap matrix $(\mathbb{X}^\dagger\mathbb{X})_{ab}$ is

$$\mathbb{X}_{ia}^\star\mathbb{X}_{ib} = (d_a - d_a^2)\delta_{ab} \tag{2.28}$$

where we used the result of Lemma 1. $\square$

Lemma 3. *If $\mathbb{M}_{ab}$ has an eigenvalue d_a different than 0 and 1, then $\mathbb{M}_{ij}$ has an eigenvalue $d_i = 1 - d_a$.*

Proof. We showed that whenever eigenvector $\mathbb{U}_{ba}$ corresponds to eigenvalue d_a that is not 1 nor 0, a vector $\mathbb{M}_{kb}\mathbb{U}_{ba}$ is nontrivial. Therefore,

$$\mathbb{M}_{lb}\mathbb{U}_{ba} = \mathbb{M}_{lk}\mathbb{M}_{kb}\mathbb{U}_{ba} + \mathbb{M}_{cb}\mathbb{M}_{lc}\mathbb{U}_{ba} = \mathbb{M}_{lk}\mathbb{M}_{kb}\mathbb{U}_{ba} + d_a\mathbb{M}_{lc}\mathbb{U}_{ca}, \tag{2.29}$$

hence,

$$\mathbb{M}_{lk}\left[\mathbb{M}_{kb}\mathbb{U}_{ba}\right] = (1 - d_a)\left[\mathbb{M}_{lb}\mathbb{U}_{ba}\right]. \tag{2.30}$$

Clearly, $\mathbb{M}_{kb}\mathbb{U}_{ba}$ must be parallel to vector $\mathbb{V}_{ki}$ if it corresponds to eigenvalue $d_i = 1 - d_a$ and orthogonal to all other vectors $\mathbb{V}_{kj}$. $\square$

Now, we are in position to show that the set of fragment, bath and core states form a complete set of states of the problem. First, we note that fragment states obtained from either hole or particle orbitals are orthogonal to bath and core states due to orthogonality of the projectors. Moreover, the hole (particle) bath states are orthogonal to each other and the hole (particle) core states due to unitarity of $\mathbb{V}$ ($\mathbb{U}$). The orthogonality of particle and hole core states follows from lemma 3. It is then sufficient to show that each hole fragment state is parallel to one fragment state obtained from particle orbitals. Indeed,

$$\langle f_a | f_i \rangle = \frac{1}{\sqrt{d_i d_a}} \mathbb{V}_{ki}^\star \mathbb{M}_{kb} \mathbb{U}_{ba}, \tag{2.31}$$

according to lemma 3 is 0 unless $d_i = 1 - d_a$ and there is a one to one correspondence between eigenvalues d_i and d_a; there can be therefore only one vector in each set that can satisfy this condition. Because those vectors are parallel and normalized, they cannot differ by more than a phase. Analogous discussion follows for bath states.

2.A.2 Mean-field density matrix in the embedding basis

Let us consider a lattice density matrix γ_0 that has been projected onto the embedding (fragment and bath) basis,

$$\gamma_0 = \begin{pmatrix} \gamma_0^{FF} & \gamma_0^{FB} \\ \gamma_0^{BF} & \gamma_0^{BB} \end{pmatrix} \tag{2.32}$$

The FF takes the form

$$(\gamma_0^{FF})_{ij} = \frac{\mathbb{V}_{ki} \mathbb{M}_{mk} \mathbb{M}_{lm} \mathbb{V}_{lj}^\star}{\sqrt{d_i d_j}} = \delta_{ij} d_i. \tag{2.33}$$

Analogous straightforward calculations follow for the other blocks. Finally

$$\gamma_0 = \begin{pmatrix} d & \sqrt{d(1-d)} \\ \sqrt{d(1-d)} & 1-d \end{pmatrix}. \tag{2.34}$$

One can now verify that the mean-field density matrix remains idempotent in the embedding basis. On the other hand, the FF block is not as it eigenvalues are expressed by the eigenvalues of the $\mathbb{M}_{ij}$ matrix. Additionally, we point out that upon unitary transformation of fragment states to the on-site basis, the trace is invariant. Therefore, we conclude that the trace of $\mathbb{M}_{ij}$ is the average number of electrons per fragment in the mean-field solution of the full system.

2.A.3 Commutativity of the mean-field and the Fock matrix in the embedding basis

Let us consider the mean-field Fock matrix in the embedding basis, f. Since γ_0 and f are hermitian, they commute if and only if their product $t = f\gamma$ is hermitian. Since t and f have the same block structure as γ_0 (Eq. 2.32), we can investigate one block at the time. And so,

$$t_{ij}^{\mathrm{FF}} = f_{ij}^{\mathrm{FF}} d_j + f_{ij}^{\mathrm{FB}}\sqrt{d_j(1-d_j)} = \sqrt{d_i d_j}\left(V_{kj}^{\star}\epsilon_k V_{ki}\right), \tag{2.35}$$

where ϵ_k is an eigenvalue of the full system Fock matrix. Similarly,

$$t_{ij}^{\mathrm{BB}} = \sqrt{(1-d_i)(1-d_j)}\left(V_{kj}^{\star}\epsilon_k V_{ki}\right). \tag{2.36}$$

The above matrices are manifestly Hermitian. Finally,

$$t_{ij}^{\mathrm{FB}} = \sqrt{d_i(1-d_j)}\left(V_{kj}^{\star}\epsilon_k V_{ki}\right) \tag{2.37}$$

and

$$t_{ij}^{\mathrm{BF}} = \sqrt{(1-d_i)d_j}\left(V_{kj}^{\star}\epsilon_k V_{ki}\right) \tag{2.38}$$

so clearly $(t^{\mathrm{FB}})_{ij}^{\star} = t_{ji}^{\mathrm{BF}}$. Therefore, t is Hermitian and f and γ_0 commute.

Chapter 3

Application of Density Matrix Embedding Theory to Realistic Extended Systems

The discussion presented in this chapter is based on our published work, see Ref. [2].

3.1 Motivation

In the previous chapter, we outlined the basics of the density matrix embedding theory and performed benchmark calculations for the one dimensional Hubbard model. For this prototypical model of strongly correlated electrons we obtained satisfactory results even with small fragment sizes. In the present chapter we wish to extend the applicability of DMET to real materials. We primarily seek to determine whether the local nature of the approximation will cause a break-down for Coulombic systems. Moreover, we investigate the applicability of less expensive impurity solvers. Indeed, the size of the primitive cells used in the present work excludes the use of exact diagonalization as an impurity solver. The ultimate goal, however, remains unchanged; we seek for approximate computational tools that allow one to access an accurate description of electronic correlation in realistic extended systems.

Just as in the Hubbard model, electron correlation plays a central role in understanding physical phenomena in extended systems. Despite significant progress recently made in applying highly accurate many-body theories to crystalline materials, [47–50] this field remains dominated by density functional theory. Even though this approach is computationally very compelling and may yield results of satisfac-

tory accuracy [51, 52], the limitations due to the approximate nature of the exchange-correlation functional still pose a challenge. [53–55]

The size-extensive wavefunction-based approaches to solids treat the system as a whole, imposing translational symmetry and Brillouin zone integration. Alternatively, numerical complexity arising from numerous degrees of freedom has been simplified, for example by means of the method of increments. [56–58] Finite order perturbation theory [59–63] and coupled cluster (CC) methods [64–66] have been formulated and implemented for extended systems. With all the previous efforts in mind, we proceed to benchmark DMET for prototypical 1-, 2-, and 3-dimensional extended systems.

3.2   Schmidt decomposition for periodic systems

Recall that DMET calculations require a definition of a suitable single particle basis that can be associated with a fragment. While in the case of the Hubbard model, the choice of the on-site basis was natural, for the case of realistic systems, such a choice is not so obvious. In the case of the present work, we employ the maximally localized Wannier functions. [67–69] These orbitals are obtained by a unitary transformation of the mean-field basis $|\psi_{n\vec{k}}\rangle$, where n is the band index and $\vec{k}$ labels the irreducible representation of the translational group. [70] This yields an orthonormal set of single particle states $|F_{\mu\vec{G}}\rangle$, where μ labels a basis in a cell $\vec{G}$. The orthonormality condition reads

$$\langle F_{\mu\vec{G}'}|F_{\nu\vec{G}}\rangle = \delta_{\mu\nu}\delta_{\vec{G}\vec{G}'}. \tag{3.1}$$

Let us be more specific at this point. First, one may replace the need of using the Wannier basis in lieu of the atomic-centered orbitals. Those orbitals are not orthogonal; one loses therefore the simplicity of the formulation of the approach. Second,

in order to form a suitable basis one must allow for mixing of the particle and hole states during the localization procedure yielding the required states. In order words, we employ the localization procedure as an affective algorithm for forming localized set of orthogonalized "atomic like" basis functions used to construct a fragment. Nonetheless, as outlined in Appendix 3.A one may constrain the indices of the bands in order to further truncate the electronic degrees of freedom. This procedure is a direct equivalence of orbital "windows" commonly used in molecular calculations where only the highest valence bands and the lowest conduction bands are treated with the correlated method.

Analogously to the fragment states, the hole states are localized to yield $|\phi_{i\vec{G}}\rangle$ orbitals which correspond to the ith hole state associated with cell $\vec{G}$. For consistency of the approach, whenever a truncation of the valence band was used in formation of the fragment states, the same level of truncation should be applied while localizing the hole states.

The Schmidt overlap matrix may now be constructed as

$$\mathbb{M}_{ij}^{\vec{G}\vec{G}'} = \sum_{\mu}\langle\phi_{j\vec{G}'}|F_{\mu\vec{0}}\rangle\langle F_{\mu\vec{0}}|\phi_{i\vec{G}}\rangle \tag{3.2}$$

where $\vec{0}$ is the reference cell constituting a fragment. In cases where more than one primitive cell is embedded, this index should be understood as the extended cell formalism. As the reader may verify, the formally infinite matrix $\mathbb{M}$ can be efficiently truncated due to the locality of the Wannier basis, $i.e.$ $\lim_{|\vec{G}|\to\infty}\langle F_{\mu\vec{0}}|\phi_{i\vec{G}}\rangle = 0$. The localization of the hole states dictates therefore a natural length scale considered in the problem. From the practical point of view, we have considered as a measure of the convergence of the truncation the overlap matrix of the embedding basis as well as the norm of the commutator of the mean-field density matrix and the Fock matrix

in the embedding basis.

Finally, let us point out that unlike the model Hamiltonian studied in the previous chapter, for the realistic systems with a multi-band basis the nontrivial eigenvalues of the $\mathbb{M}$ matrix are very close to 1 and 0 making the Schmidt decomposition numerically noisy. As this is just a technicality, we do not focus on that issue here and refer the reader to Appendix 3.A.

3.3   Impurity Hamiltonian for crystalline materials

The main difficulty in adopting DMET for realistic materials lies in the formation of the impurity Hamiltonian. For realistic systems, the physical Hamiltonian can be written as

$$\hat{H} = E_{NN} + \hat{V}_{Ne} + \hat{V}_{ee} + \hat{T} = E_0 + \hat{h} + \hat{V} \tag{3.3}$$

with E_{NN} being nuclear repulsion energy, $\hat{V}_{Ne}$ and $\hat{V}_{ee}$ the potential energy of electron-nuclei and electron-electron interactions and $\hat{T}$ the electronic kinetic energy. Those can be expressed in terms of a constant E_0 and one- and two-body operators, $\hat{h}$ and $\hat{V}$. Due to the delicate nature of Coulombic systems, the summation over the infinite number of electrostatic terms must be handled with care. The same is true for the transformation of the physical Hamiltonian to the embedding basis. In the present approach, we propose to avoid problems with electrostatic terms as follows. We start by expressing the Hamiltonian in the second quantized form with the aid of the mean-field Fock matrix (F) and density matrix (γ)

$$F_{\mu\nu} = h_{\mu\nu} + \sum_{\lambda\sigma} V_{\mu\lambda\nu\sigma}\gamma_{\sigma\lambda}, \tag{3.4}$$

as

$$\hat{H} = E_0 - \sum_{\mu\nu} F_{\mu\nu}\gamma_{\nu\mu} + \frac{1}{2}\sum_{\mu\nu\lambda\sigma} V_{\mu\lambda\nu\sigma}\gamma_{\sigma\lambda}\gamma_{\nu\mu}$$

$$+ \sum_{\mu\nu}(F_{\mu\nu} - V_{\mu\lambda\nu\sigma}\gamma_{\sigma\lambda})c_\mu^\dagger c_\nu + \frac{1}{4}\sum_{\mu\nu\lambda\sigma} V_{\mu\nu\lambda\sigma}c_\mu^\dagger c_\nu^\dagger c_\sigma c_\lambda \qquad (3.5)$$

where $E_0 = EN$ with E being the mean-field energy per unit cell and N the number of cells. Here, V is an antisymmetrized integral. Clearly, the above is just an rearrangement of the physical Hamiltonian. No approximations have yet been made. The problem of divergent terms is still present. For example, the constant $\frac{1}{2}\sum_{\mu\nu\lambda\sigma} V_{\mu\lambda\nu\sigma}\gamma_{\sigma\lambda}\gamma_{\nu\mu}$ cannot be summed independently as it has no meaningful thermodynamic limit. We propose therefore to express all quantities in Eq. 3.5 in the embedding basis first, and then perform required summations. In other words we independently transform the two-body matrix elements, Fock operator and the density matrix into the embedding basis, i.e. $F_{\mu\nu} \to \tilde{F}_{ee'}$, $\gamma_{\mu\nu} \to \tilde{\gamma}_{ee'}$ and $V_{\mu\nu\lambda\sigma} \to \tilde{V}_{ee'e''e'''}$. While the two-body elements are transformed as usual, let us write explicit form of the one-body matrix elements and the constant term. They become:

$$\tilde{h}_{ee'} = \tilde{F}_{ee'} - \sum_{e''e'''} \tilde{V}_{ee''e'e'''}\tilde{\gamma}_{e'''e''} \qquad (3.6)$$

$$\tilde{E}_0 = EN_F - \sum_{fe}\left(\tilde{F}_{fe} - \frac{1}{2}\sum_{e'e''}\tilde{V}_{fe'ee''}\tilde{\gamma}_{e''e'}\right)\tilde{\gamma}_{ef}. \qquad (3.7)$$

Again, E denotes the mean-field energy of the fragment and N_F is the number of fragments. As the reader may notice, a restriction of the summation indices was introduced to the constant term. The range of index f covers only the single particle states associated with fragment, not the full embedding basis. The reason for that will become apparent soon.

Let us stress that the above construction is an approximate way of defining the impurity Hamiltonian. This approximation is, however, well justified. As is shown

in Appendix 3.A, the mean-field density matrix projected into the embedding basis commutes with the Fock matrix projected to the embedding space, i.e. $[\tilde{F}, \tilde{\gamma}] = 0$. Moreover, $\tilde{\gamma}$ is idempotent. In our approximation, the Fock matrix of the impurity Hamiltonian constructed from $\tilde{\gamma}$ takes the form

$$F_{ee'}^{\mathrm{imp}} = \tilde{h}_{ee'} + \sum_{e''e'''} \tilde{V}_{ee''e'e'''} \tilde{\gamma}_{e'''e''} = \tilde{F}_{ee'}. \qquad (3.8)$$

It the therefore clear that the mean-field density matrix in the embedding basis is a valid solution of HF equations for the impurity Hamiltonian as defined above. Moreover, the energy of the fragment computed according to Eq. 2.10 reduces to EN_F; hence we must conclude that employing Hartree-Fock as an impurity solver yields the energy equivalent to the full lattice problem. It it important to note that the effective potential required to achieve DMET convergence criterion was set to 0 in the demonstration above. In the case where a method capable of accounting for electron correlation is employed, the solution to DMET equations will require a non-zero effective potential. As this works constitutes a first application of the DMET procedure to crystalline material, we choose a minimalistic approach to the convergence criterion. In what follows, the effective potential is not only diagonal, but also independent on the sites. Therefore, in the full lattice problem it acts as a chemical potential which cannot change the HF solution. We do not need therefore to resolve the HF problem during the optimization procedure as the mean-field density remains constant. As a consequence, the suitable convergence criterion is that the average number of electrons in the fragment carried in the correlated wavefunction agrees with the physical electron number of the fragment. Once again, for the periodic system the average number of electrons per unit cell is known and well defined. Due to the simplification, we denote calculations in the present chapter as DET for sake of consistency with the previous chapter.

3.4   Impurity Solver

As the size of the many-body Hilbert spaces considered in the present work exceeds
the feasibility of solving the impurity Hamiltonian exactly, in this work we tackle
the problem with coupled cluster methods. In this approach [25], the ansatz for the
ground state wavefunction can be expressed as

$$|\Psi\rangle = e^{\hat{T}}|0\rangle, \tag{3.9}$$

where $|0\rangle$ is a Slater determinant and $\hat{T}$ is a cluster operator

$$\hat{T} = \hat{T}_1 + \hat{T}_2 + \hat{T}_3 \ldots \tag{3.10}$$

with $\hat{T}_n$ being a n-tuple excitation operator, for example,

$$\hat{T}_2 = t_{ij}^{ab} a^{\dagger} b^{\dagger} ji \tag{3.11}$$

where indices a and b denote particle and i and j hole states. In the typical imple-
mentation the CC equations are solved in a projective manner. The first step involves
a truncation of the cluster operator to a given level of excitations. In practical ap-
plications, only the $\hat{T}_1$ and $\hat{T}_2$ operators are retained, giving rise to coupled cluster
single and double excitations (CCSD). Alternatively, one may neglect also the single
excitation operator which is known as coupled cluster with double excitations (CCD).
Then, the physical Hamiltonian undergoes similarity transformation

$$\bar{H} = e^{-\hat{T}} \hat{H} e^{\hat{T}} \tag{3.12}$$

and is projected onto a truncated Hilbert space spanned by the reference determinant
$|0\rangle$ and all excited determinants with the excitation level commensurate with the
elements of the cluster operator retained. Defining $|Z\rangle$ as a representation of the

projective subspace of excited determinants, the matrix representation of the CC (non-hermitian) Hamiltonian takes the form

$$\hat{H} = \begin{pmatrix} \langle 0|\bar{H}|0\rangle & \langle 0|\bar{H}|Z\rangle \\ \langle Z|\bar{H}|0\rangle & \langle Z|\bar{H}|Z\rangle \end{pmatrix}. \tag{3.13}$$

The excitations amplitudes are then solved subject to the constraint that a vector

$$\begin{pmatrix} 1 \\ 0 \end{pmatrix} \tag{3.14}$$

is a right eigenvector of the CC Hamiltonian in the projective space, i.e.

$$\begin{pmatrix} \langle 0|\bar{H}|0\rangle & \langle 0|\bar{H}|0\rangle \\ \langle Z|\bar{H}|0\rangle & \langle Z|\bar{H}|Z\rangle \end{pmatrix} \begin{pmatrix} 1 \\ 0 \end{pmatrix} = E \begin{pmatrix} 1 \\ 0 \end{pmatrix}. \tag{3.15}$$

This yields an energy expression $E = \langle 0|\bar{H}|0\rangle$ with the constraints $\langle Z|\bar{H}|0\rangle = 0$ for every determinant in the projective subspace. Defining an operator

$$\hat{Z} = \hat{Z}_1 + \hat{Z}_2 + \ldots \tag{3.16}$$

with, for example, $\hat{Z}_2 = z_{ab}^{ij} i^\dagger j^\dagger ba$, the above can be written in the term of CC Lagrangian,

$$\mathcal{L}[t,z] = \langle 0|(1+\hat{Z})\bar{H}|0\rangle. \tag{3.17}$$

Now, the equations for the t-amplitudes can be expressed as

$$\frac{\partial \mathcal{L}[t,z]}{\partial z_{ab}^{ij}} = 0. \tag{3.18}$$

While the numerical values or the z-amplitudes are irrelevant from the point of view of the energy, it is conceptually useful to view $\langle 0|(1+\hat{Z})$ as the eigenbra of the CC Hamiltonian in the projective space [71,72] with the z-amplitudes defined by requiring

$$\frac{\partial \mathcal{L}[t,z]}{\partial t_{ij}^{ab}} = 0. \tag{3.19}$$

With the above bi-orthogonal framework, the necessary density matrices required in DMET approach can be computed as [73]

$$\gamma_{pq} = \langle 0 | (1 + \hat{Z}) e^{-\hat{T}} q^{\dagger} p \, e^{T} | 0 \rangle \tag{3.20}$$

$$\Gamma_{pqrs} = \langle 0 | (1 + \hat{Z}) e^{-\hat{T}} r^{\dagger} s^{\dagger} qp \, e^{T} | 0 \rangle. \tag{3.21}$$

The above constitutes the so called "CC expectation value" [73] which we deem correct for the purposes of DMET. We therefore did not include the orbital relaxation term contribution to the density matrices.

3.5 Application to crystalline materials

3.5.1 Computational details

The construction of Wannier functions was implemented in Gaussian Developement Version [74] that was also used to perform the periodic HF calculations. The spin symmetry was preserved. The localization of crystalline orbitals was performed by adapting the scheme of Ref. [75] where the Boys localization is replaced by Pipek-Mezey localization [68] with Löwdin population [69]. For 1D systems, we used a $\vec{k}$-point mesh of at least 400 points; for 2D and 3D 400 and 70000 $\vec{k}$-points were used, respectively.

Due to linear-dependencies in the HF calculations, the most diffuse basis functions of the 6-31G basis [76,77], were changed to 0.35, 0.30 and 0.20 for the carbon, nitrogen and boron atoms, respectively.

In all calculations, the threshold for the retaining of the bath states was set to 10^{-6}. The fragment states corresponding to eigenvalues that were closer to 1 or 0 than this threshold were constructed according to the formalism outlined in Appendix 3.A.

3.5.2   1D carbon system

Here we benchmark the DET approximation against three carbon polymers, polyyne $(C\equiv C)_{\infty}$, polyacetylene $(CH=CH)_{\infty}$, and polyethylene $(CH_2-CH_2)_{\infty}$. In the present work, we adopt the geometries from Ref. [66]. The geometrical parameters are $r_{C\equiv C} = 1.263\mathring{A}$, $r_{C-C} = 1.132\mathring{A}$ for polyyne, $r_{C=C} = 1.369\mathring{A}$, $r_{C-C} = 1.426\mathring{A}$, $r_{C-H} = 1.091\mathring{A}$, $\angle_{C=C-C} = 124.5°$, $\angle_{C=C-H} = 118.3°$ for polyacetylene, and $r_{C-C} = 1.534\mathring{A}$, $r_{C-H} = 1.100\mathring{A}$, $\angle_{C-C-C} = 113.7°$, $\angle_{H-C-H} = 106.1°$ for polyethylene. In order to gain better insight into the performance of the DET approximation, we additionally deform the above systems by keeping all variables, apart from the carbon-carbon bonds, fixed, while scaling the carbon-carbon bonds uniformly with a parameter α. In all calculations, the $1s$ orbitals of carbon were eliminated from consideration in DET and coupled cluster calculations. $DET(n)$ denotes calculations with n unit cells used as a fragment. The benchmark data (Extr) was obtained by extrapolating the correlation (E_{corr}) of given method, i.e.,

$$E_{Extr} = E_{HF} + E_{corr}(n) - E_{corr}(n-1) \qquad (3.22)$$

E_{HF} is the HF energy per unit cell of infinite system and n denotes the number of monomers in the oligomer used for the extrapolation. We found that a satisfactory accuracy of extrapolation was achieved with $n \approx 9$.

Polyyne

Let us begin with the most challenging system for the embedding calculations, polyyne. In this case, one expects the slowest decay of the correlation energy contributions from further cells to the unit cell. [66] The results of the calculations with STO-3G basis are presented in Fig. 3.5.1. Clearly, even for the calculations with a single unit cell,

the CCD and CCSD impurity solvers provide a reasonable description of the system for almost all values of the stretching parameter α. The discrepancy with respect to the oligomeric extrapolation does not exceeds 10 mE_h which accounts for roughly 5% difference in the correlation energy. Extending the embedded fragment to two unit cells further improves the agreement with the thermodynamic limit and tends to make the discrepancy fairly independent on the value of the parameter α. Importantly, the DET embedding correctly predicts the carbon-carbon bond elongation due to the inclusion of the electron correlation effects which impacts the optimal value of parameter α.

The qualitative and quantitative agreement between the extrapolated and DET results remain valid with the larger basis set as well. The data for the 6-31G basis are presented in Fig. 3.5.2. The absolute discrepancy between those two approaches do increase, but so does the magnitude of the correlation energy. The overall shape of the energy profile is properly reproduced as is the bond elongation due to the correlation effects.

Let us also comment on the size of the impurity space. For the fragment of 1 unit cell taken as a fragment there are 8 fragment and 8 bath states with 16 electrons present in the impurity problem. One can therefore clearly recognize the efficiency of the current embedding scheme in truncating the single particle Hilbert space of the problem.

Polyacetylene

Let us now turn the attention to polyacetylene. The results of the calculations with DET embedding with STO-3G basis are presented in Fig. 3.5.3. Analogously as in the case of polyyne, the agreement between the DET energy profile and the ex-

Figure 3.5.1 : Energy per unit cell profile for polyyne $(C\equiv C)_\infty$ with respect to uniform deformation (see text for details) with the STO-3G basis. The DET(1) and DET(2) results with CCSD(left panel) and CCD(right panel) as the impurity solver are compared to corresponding CCSD and CCD oligomeric extrapolations (Extr) and Hartree-Fock (HF). The bottom insets shows the difference between DET and extrapolated data. Figure taken from Ref. [2].

Figure 3.5.2 : Energy per unit cell profile for polyyne $(C\equiv C)_\infty$ with respect to uniform deformation (see text for details) with the 6-31G basis. The DET(1) results with CCSD(left panel) and CCD(right panel) as the impurity solver are compared to corresponding CCSD and CCD oligomeric extrapolations (Extr) and Hartree-Fock (HF). The bottom insets shows the difference between DET and extrapolated data. Figure taken from Ref. [2].

trapolated one is more than satisfactory. The single unit cell embedding is virtually indistinguishable for the extrapolated data on the energy scale of the figure. Enlarging the fragment to two unit cells brings the error to almost 0 over the entire range of the parameter α considered. With the increased basis set size, (see Fig. 3.5.4) the extrapolated and embedded results can be told apart, especially for very contracted systems ($\alpha \leq 0.95$), but the difference is not large. The error in the correlation energy is roughly 5 mE_h. The extrapolated data and the embedding data lead to the same conclusions: electron correlation effects in this system favour the elongated carbon-carbon bonds.

Again, in order to give the reader a feeling of the dimension of the impurity problem, the single cell STO-3G calculation describes merely 20 electrons in 20 orbitals.

Polyethylene

The last system under investigation in this section is polyethylene. In this case, the STO-3G DET(1) (see Fig. 3.5.5), coincides very well with the extrapolated data. In particular, the CCD impurity solver yields an energy profile that almost completely overlaps with the extrapolated data. Regardless, the CCSD and CCD DET(2) calculations improve further on the quality of the data. In both cases, the discrepancy between the embedded and extrapolated energy profile becomes virtually 0. The calculations involving larger basis, presented in Fig. 3.5.6, one again observe some sort of minor discrepancy between two curves, especially for more contracted systems. The physics, however, remains correct. The correlation contribution to the unit cell energy tends to shift the lengths of the carbon bonds towards larger values, yet the impact is noticeably smaller than in the case of conjugated polymers.
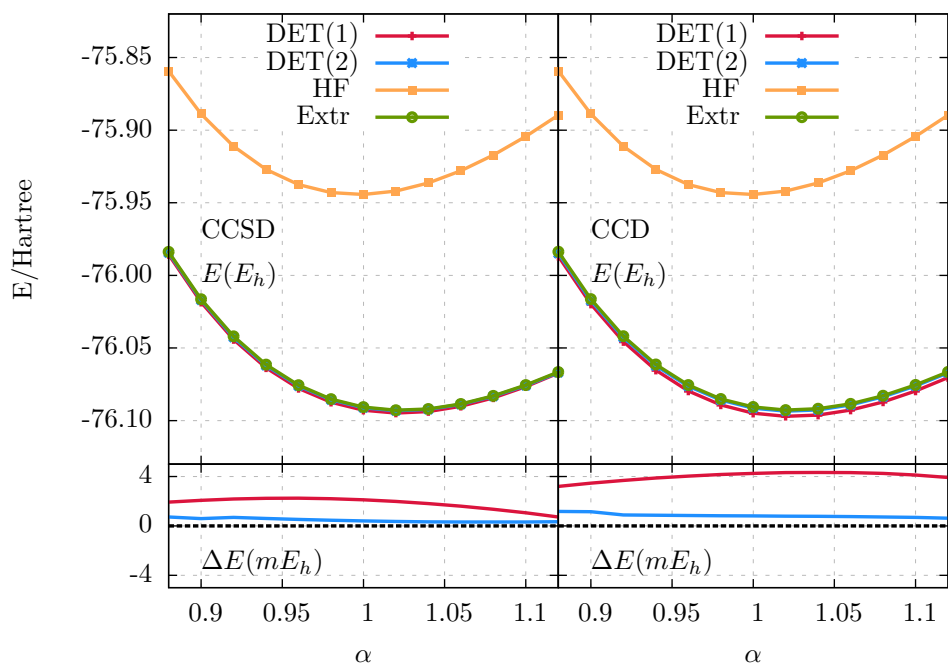
Figure 3.5.3 : Energy per unit cell profile for polyacetylene $(CH=CH)_\infty$, with respect to uniform deformation (see text for details) with the STO-3G basis. The DET(1) and DET(2) results with CCSD(left panel) and CCD(right panel) as the impurity solver are compared to corresponding CCSD and CCD oligomeric extrapolations (Extr) and Hartree-Fock (HF). The bottom insets shows the difference between DET and extrapolated data. Figure taken from Ref. [2].
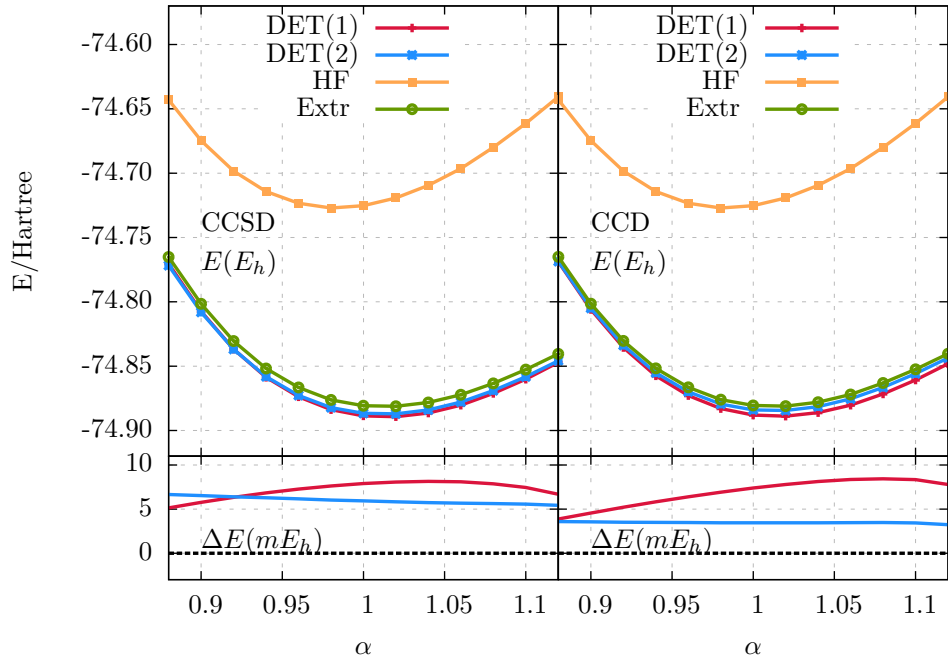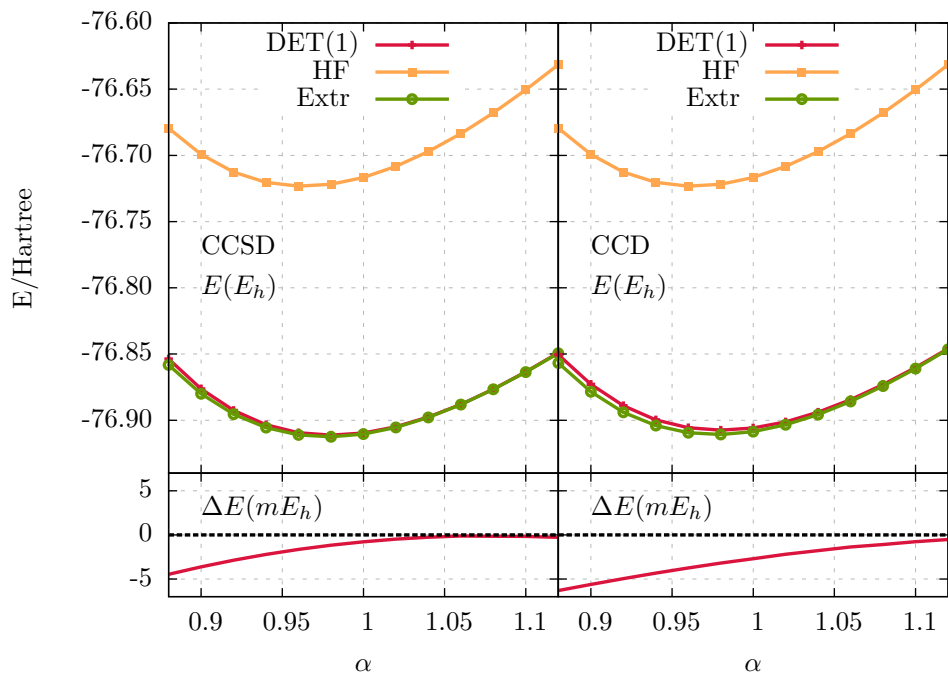
Figure 3.5.4 : Energy per unit cell profile for polyacetylene $(CH=CH)_{\infty}$, with respect to uniform deformation (see text for details) with the 6-31G basis. The DET(1) results with CCSD(left panel) and CCD(right panel) as the impurity solver are compared to corresponding CCSD and CCD oligomeric extrapolations (Extr) and Hartree-Fock (HF). The bottom insets shows the difference between DET and extrapolated data. Figure taken from Ref. [2].
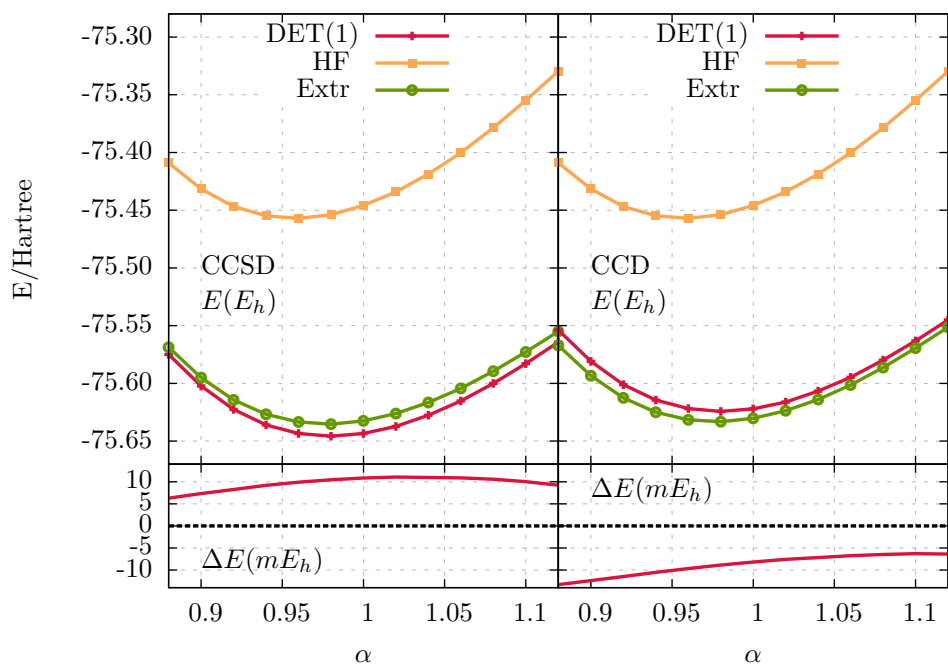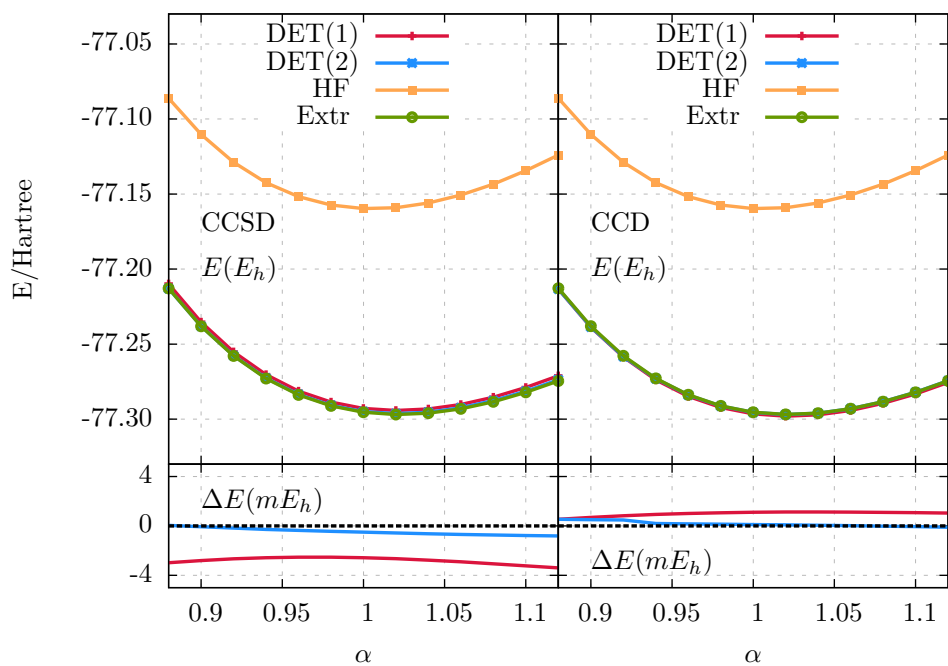
Figure 3.5.5 : Energy per unit cell profile for polyethylene $(CH_2 = CH_2)_\infty$, with respect to uniform deformation (see text for details) with the STO-3G basis. The DET(1) and DET(2) results with CCSD(left panel) and CCD(right panel) as the impurity solver are compared to corresponding CCSD and CCD oligomeric extrapolations (Extr) and Hartree-Fock (HF). The bottom insets shows the difference between DET and extrapolated data. Figure taken from Ref. [2].
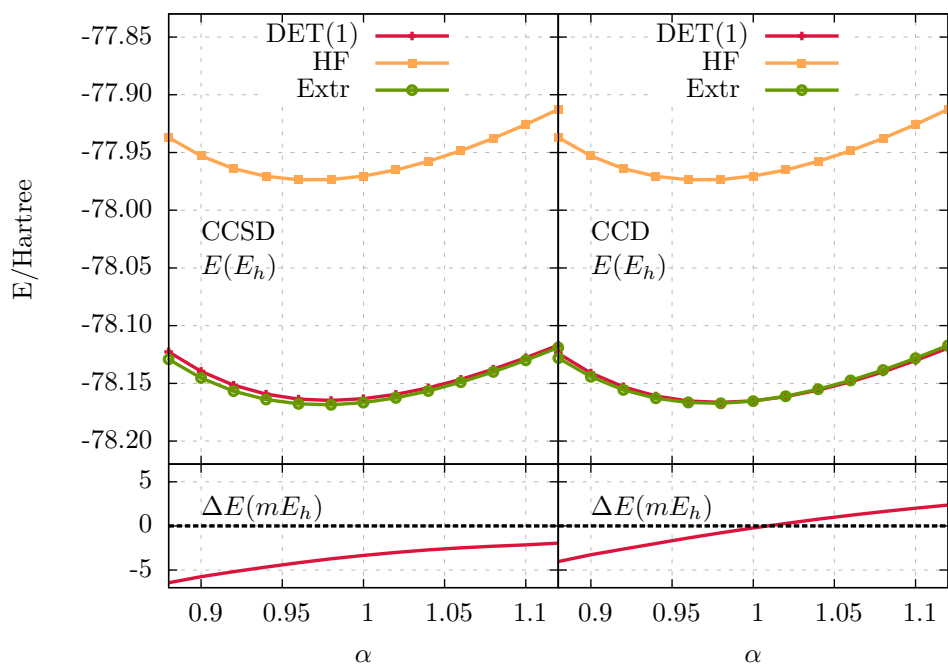
Figure 3.5.6 : Energy per unit cell profile for polyethylene $(CH_2-CH_2)_\infty$, with respect to uniform deformation (see text for details) with the 6-31G basis. The DET(1) results with CCSD(left panel) and CCD(right panel) as the impurity solver are compared to corresponding CCSD and CCD oligomeric extrapolations (Extr) and Hartree-Fock (HF). The bottom insets shows the difference between DET and extrapolated data. Figure taken from Ref. [2].

3.5.3   2D and 3D: boron nitride and diamond

Having established that the DET approach yields a correct description of the correlation energy in 1D systems, we now turn our attention 2D and 3D materials, where the extrapolation may not be feasible. For the purpose of demonstration, we attempt to study an model of infinitely separated sheets of hexagonal BN, [78, 79] and diamond. In both cases, the single-cell embedding calculations were performed with the two lowest bands excluded from consideration.

In Fig 3.5.7 we present the dependence of the energy density as a function of the translational vector defining the 2D lattice. Clearly, the inclusion of electron correlation effects has a significant impact on the predicted optimal structure with both CCD and CCSD impurity solvers. We note, however, that the predicted lattice constant is somewhat larger than the one reported in the literature for hexagonal BN. [80] Whether this effect can be explained by not including a solid substrate, by treating only one sheet of BN, or by the limited size of the basis set is beyond the scope of the current study. The point we should stress is that the embedding scheme presented allows us to fold the tremendous single particle Hilbert space into a small impurity Hamiltonian. Moreover, the size of the impurity Hamiltonian does not depend of the dimensionality of the material. Indeed, the dimension of the problem one actually solves for the BN is the same as for polyyne, i.e., 16 electrons in 16 orbitals for STO-3G and 32 electrons in 32 orbitals for 6-31G.

The calculations for the 3D diamond structure are presented in Fig. 3.5.8. Again, even with the smaller STO-3G basis, the reader may observe that the electron correlation effects tend to favour a larger translational vector as compared to Hartree-Fock calculations. We do not present any sort of quantitative discussion of the data presented here as it would require using larger basis sets. The main point remains;
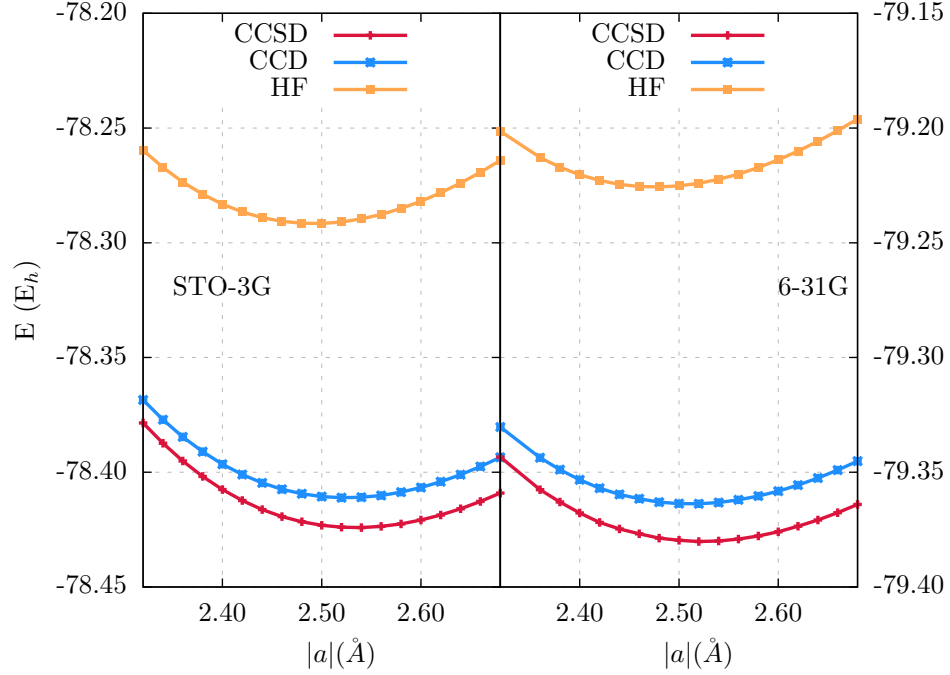
Figure 3.5.7 : Energy per unit cell of honeycomb BN lattice as a function of lattice parameter. The DET(1) calculations with CCSD and CCD impurity solvers are compared with the HF for the STO-3G (left panel) and the 6-31G basis (right panel). Figure taken from Ref. [2].

the Hilbert space of the impurity Hamiltonian is the same as in the case of BN and polyyne, despite the fact that we describe a 3D system.

3.6   Conclusions

In this chapter we presented the first application of the density matrix embedding theory for realistic periodic systems. We proposed a way of preparing the impurity Hamiltonian that mitigates the problem of Coulombic sums and performing the Schmidt decomposition of Slater determinants describing infinite systems. While we have benchmarked the approach with the coupled cluster based impurity solver, we
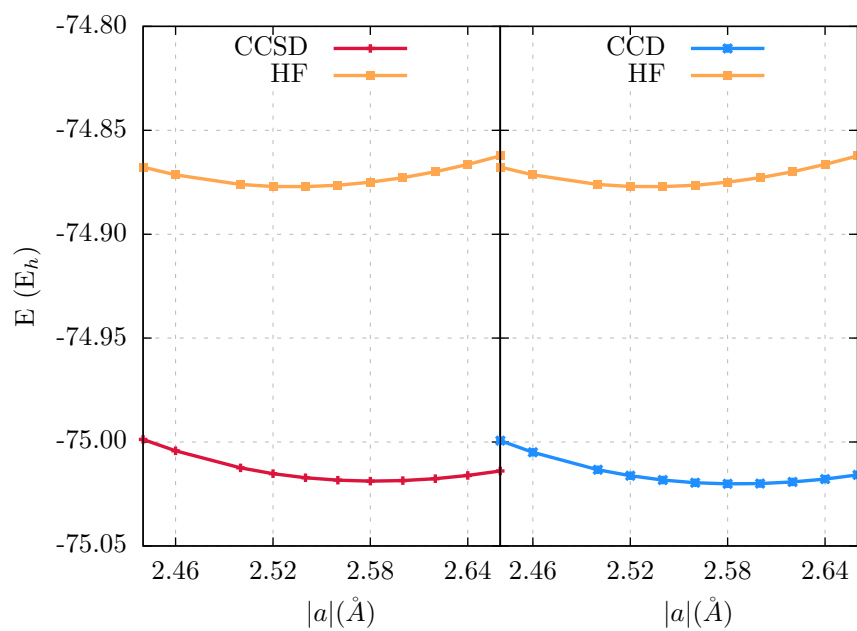
Figure 3.5.8 : Energy per unit cell of diamond as a function of lattice parameter. The DET(1) calculations with CCSD (left panel) and CCD (right panel) impurity solvers are compared with the HF for the STO-3G basis set. Figure taken from Ref. [2].

must stress that the approach can be combined with any impurity solver.

The current approach was benchmarked against realistic 1D models with satisfactory quantitative agreement with the oligomeric extrapolations. We should, however, stress that even though the description offered by these two approaches agree, the nature of the problem is quite different. In the oligomeric extrapolation, the coupled cluster treats the excitations over the entire lattice whereas in DMET or DET, the coupled cluster treats an effective Fock space calculation of the fragment with the electron reservoir mimicked by the bath.

We should note that DMET, despite being quite a recent model, seems to be capable of providing accurate and computationally affordable description of extended systems with a significantly truncated single particle Hilbert space. We hope that this chapter helps to support the confidence in the predictive power of the method.

Appendix

3.A   Handling band truncation and the disentangled states

In the following, we outline more details on how the formation of bath and fragment states was performed in the present study. The discussion here is based on Ref. [2]. The indices p and q denote hole states.

3.A.1   Fragment states with truncated bands

In order to fix the notation, we note that both, Bloch and Wannier representations are normalized according to

$$\langle \psi_{i\vec{k}} | \psi_{j\vec{k}'} \rangle = \delta_{ij} \delta_{\vec{k}\vec{k}'}$$

$$\langle \phi_{i\vec{G}} | \phi_{j\vec{G}'} \rangle = \delta_{ij} \delta_{\vec{G}\vec{G}'}, \qquad (3.23)$$

and are related by the discrete Fourier relation [67]

$$|\phi_{i\vec{G}}\rangle = \frac{1}{\sqrt{N}} \sum_{\vec{k}} e^{-i\vec{k}\cdot\vec{G}} \sum_{j} \mathbb{U}_{ji}^{\vec{k}} |\psi_{j\vec{k}}\rangle, \qquad (3.24)$$

where N is the number of unit cells. The density matrix becomes

$$\hat{\gamma} = \sum_{p\vec{k}} |\psi_{p\vec{k}}\rangle\langle\psi_{p\vec{k}}| = \sum_{p\vec{G}} |\phi_{p\vec{G}}\rangle\langle\phi_{p\vec{G}}| = \sum_{p'} |\phi_{p'}\rangle\langle\phi_{p'}|, \qquad (3.25)$$

where index p denotes hole states at given $\vec{k}$ or labeled by cell index $\vec{G}$, whereas in the last term $p' = (p\vec{G})$ denotes all hole states in all cells.

The orthonormal single-particle basis $|F_{i\vec{G}}\rangle$ becomes

$$|F_{i\vec{G}}\rangle = \frac{1}{\sqrt{N}} \sum_{\vec{k}} e^{-i\vec{k}\cdot\vec{G}} \sum_j \mathbb{U}_{ji}^{\vec{k}} |\psi_{j\vec{k}}\rangle, \tag{3.26}$$

with index j running over the chosen subset of bands. Because the states $F_{i\vec{G}}$ are orthogonal to the states not included in the localization procedure, such states do not overlap with the localized basis define above. To simplify notation, the summation over hole states can be therefore carried out over the entire range.

It now clear that the one particle density matrix in the embedding basis admits the blocked structure

$$\tilde{\gamma} = \begin{pmatrix} \gamma^{\mathrm{FF}} & \gamma^{\mathrm{FB}} \\ \gamma^{\mathrm{BF}} & \gamma^{\mathrm{BB}} \end{pmatrix} = \begin{pmatrix} d & \sqrt{d(1-d)} \\ \sqrt{d(1-d)} & 1-d \end{pmatrix}, \tag{3.27}$$

where d is the diagonal matrix with entries being the non-zero eigenvalues of $\mathbb{M}$.

Again, the Fock matrix projected onto embedding basis commutes with the density matrix in the embedding basis, which one can show by studying matrix $t = \tilde{F}\tilde{\gamma}$ which turns to be Hermitian.

The fragment-fragment block reads,

$$\begin{aligned} t_{ij}^{\mathrm{FF}} &= \tilde{F}_{ij}^{FF} d_j + \tilde{F}_{ij}^{FB} \sqrt{d_j(1-d_j)} \\ &= \sqrt{d_i d_j} \sum_{pq} \mathbb{V}_{pi} \langle \psi_p | \hat{F} | \psi_q \rangle \mathbb{V}_{qj}^{\star} = [t_{ji}^{\mathrm{FF}}]^{\star}, \end{aligned} \tag{3.28}$$

where $\hat{F}$ is the crystal Fock operator. We have used the fact that a vector $\hat{F}|\phi_q\rangle$ does not contain contributions from particle states. Hence it can be written as $\sum_r |\phi_r\rangle\langle\phi_r|\hat{F}|\phi_q\rangle$ with indices q and r being the hole states. Similarly,

$$t_{ij}^{\mathrm{BB}} = \sqrt{(1-d_i)(1-d_j)} \sum_{pq} \mathbb{V}_{pi} \langle \phi_p | \hat{F} | \phi_q \rangle \mathbb{V}_{qj}^{\star} = [t_{ji}^{\mathrm{BB}}]^{\star}$$

$$t_{ij}^{\mathrm{FB}} = \sqrt{d_i(1-d_j)} \sum_{pq} \mathbb{V}ri \langle \phi_p | \hat{F} | \phi_q \rangle \mathbb{V}_{qj}^{\star} = [t_{ji}^{\mathrm{BF}}]^{\star}. \tag{3.29}$$

3.A.2   Handling disentangled states

Here, we propose a way of constructing fragment states that would correspond to very small eigenvalues of the Schmidt overlap matrix. We assume that the eigenvalues differ from 0 or 1 by an arbitrarily small value. Let us consider that there exists a set of eigenvalues d that are close to 1. In such a case, we propose to remove the bath state and retain a modified fragment state that takes the form

$$|\tilde{f}_i\rangle = \sum_p \mathbb{V}^{\star}_{pi}|\phi_p\rangle. \tag{3.30}$$

Because $\mathbb{V}$ is unitary, these states are orthonormal and orthogonal to all other fragment and bath states. Additionally, the density matrix in such a basis is expressed as,

$$\tilde{\gamma} = \begin{pmatrix} d & \sqrt{d(1-d)} & 0 \\ \sqrt{d(1-d)} & 1-d & 0 \\ 0 & 0 & 1 \end{pmatrix}, \tag{3.31}$$

where the last block corresponds to the basis $|\tilde{f}\rangle$. With such a definition, the density matrix in the embedding basis remains idempotent and one could also easily verify that it commutes with Fock matrix in the embedding basis.

In the case where the eigenvalues d are close to 0, we propose to construct an auxiliary matrix $\mathbb{N}$,

$$\mathbb{N}_{kl} = \langle F_l|\Big(\mathbb{I} - \sum_p |\phi_p\rangle\langle\phi_p|\Big)|F_k\rangle. \tag{3.32}$$

This matrix can be decomposed as $\mathbb{N} = \mathbb{U}\lambda\mathbb{U}^{\dagger}$. Let us demonstrate that for every eigenvalue d_i of $\mathbb{M}$ different from 0, $\mathbb{N}$ has eigenvalue $1 - d_i$. One can define a column vector $\mathbb{U}^{\star\prime}_{ki} = \sum_q \langle F_k|\phi_q\rangle\mathbb{V}^{\star}_{qi}$ with a norm $\sum_k \mathbb{U}^{\prime\star}_{ki}\mathbb{U}^{\prime}_{ki} = d_i$. This vector is therefore

a non-trivial vector whenever d_i is not an exact zero. One may also check that $\sum_k \mathbb{N}_{lk}\mathbb{U}'_{ki} = (1 - d_i)\mathbb{U}'_{li}$.

We suggest that one could replace a fragment state $|f_i\rangle$ corresponding to an eigenvalue close to 0, with the state

$$|\bar{f}_i\rangle = \sum_k \frac{\mathbb{U}^\star_{ik}}{\sqrt{\lambda_i}}\Big(\mathbb{I} - \sum_p |\phi_p\rangle\langle\phi_p|\Big)|F_k\rangle, \tag{3.33}$$

with eigenvalue $\lambda_i = 1 - d_i$ and neglect a bath state entangled with $|f_i\rangle$. We now show that $\bar{f}_i$ corresponding to eigenvalue λ_i is orthogonal to all fragment states $|f_j\rangle$ corresponding to d_j not equal to $1 - \lambda_i$, that is,

$$\langle f_j|\bar{f}_i\rangle = \frac{1 - d_j}{\sqrt{d_j\lambda_i}}\sum_{kp} \mathbb{V}_{pj}\langle\phi_p|F_k\rangle\mathbb{U}^\star_{ki}$$

$$= \frac{\lambda_i}{\sqrt{d_j\lambda_i}}\sum_{kp} \mathbb{V}_{pj}\langle\phi_p|F_k\rangle\mathbb{U}^\star_{ki} \tag{3.34}$$

must vanish whenever $\lambda_i \neq 1 - d_j$. Analogously, for the bath states not associated with fragment $|f_j\rangle$,

$$\langle b_j|\bar{f}_i\rangle = -\sqrt{\frac{d_j}{1 - d_j}}\langle f_j|\bar{f}_i\rangle. \tag{3.35}$$

The orthogonality to states $|\tilde{f}_i\rangle$ (Eq. 3.30) also holds. The density matrix in the basis defined above admits the form

$$\tilde{\gamma} = \begin{pmatrix} d & \sqrt{d(1-d)} & 0 & 0 \\ \sqrt{d(1-d)} & 1-d & 0 & 0 \\ 0 & 0 & 1 & 0 \\ 0 & 0 & 0 & 0 \end{pmatrix}. \tag{3.36}$$

Again, this matrix remains idempotent and the commutation relations with the Fock operator are preserved. (one again uses the fact that $\hat{F}|\phi_p\rangle = \sum_q |\phi_q\rangle\langle\phi_q|\hat{F}|\phi_p\rangle$ to show that $\langle\bar{f}_i|\hat{F}|\phi_p\rangle = 0$).

The density matrix above traces to the integer number of particles and dictates the number of electrons we include in the impurity problem. Let us note, however, that such truncation may violate the average number of electrons in the fragment. Nonetheless, the error is proportional to a cutoff used to determine whether given eigenvalue is close to 0 and 1.

Chapter 4

Towards lower scaling impurity solvers: unconventional Coupled Cluster Methods

The efforts towards accounting for electron correlation in the extended systems described so far were focused on the development of the quantum embedding theory. The main focus was put on the formation of the impurity problem and investigating its properties. The impurity Hamiltonian was, however, solved either exactly, or with the aid of well-established approaches such as conventional coupled cluster. Despite the fact that the description of the correlation energy was more than satisfactory even with very small fragments, more realistic calculations with the embedding of many unit cells may be beyond the reach of the impurity solvers employed. In the present chapter we therefore shift the focus to investigate the possibility of developing a robust and accurate many-body approaches that allows us to study larger-scale problems. The aim of this chapter is to formulate a technique that is capable of efficient treatment of strong correlation: the pair coupled cluster method. By analyzing its success, we provide insights on how to generalize this approach towards robust tools that allow for balanced description of the total correlation energy.

The discussion presented in this chapter is based on our published work, see Ref. [3] and Ref. [5].

4.1 The concept of seniority

The cornerstone of pair coupled cluster doubles (pCCD) is the concept of seniority. Its definition is very simple: the seniority of a determinant is the number of unpaired electrons. In other words, each spinorbital ϕ_i is paired with another orbital $\phi_{\bar{i}}$ and the total number of paired orbitals which contain only one electron between them defines a seniority number. A given mapping connecting a given spinorbital to its partner is called a paring scheme. For the purpose of this work, we shall consider only a paring scheme where an α-orbital is connected to a β-orbital that has the same spatial form. The seniority operator Ω is then

$$\hat{\Omega} = \hat{N} - 2\hat{D}, \tag{4.1}$$

where $\hat{N}$ is the number operator and $\hat{D}$ is the double occupancy operator. As the reader may easily notice, the double occupancy operator $\hat{D} = \sum_i n_{i\uparrow} n_{i\downarrow}$ is not invariant to a unitary transformation of the basis defining the local number operators n_i. For example, a HF determinant is an eigenfunction of individual the n_i operators in the canonical basis, which does not have to be true in the case where the n_i operators are expressed in the on-site basis.

The question the reader may ask, however, is why may the seniority be important. Generally, the seniority operator does not commute with the Hamiltonian (apart from some spacial cases such as the reduced paring Hamiltonain [7]) so it cannot be used to block-diagonalize it. Moreover, the very idea of seniority depends on the arbitrary choice of the paring scheme. While the above is true, the seniority number can be used as a convenient way of organizing the Hilbert space of the problem.

In the conventional approach to many-body problems in quantum chemistry, one usually starts with a reference determinant and parametrizes Hilbert space in terms
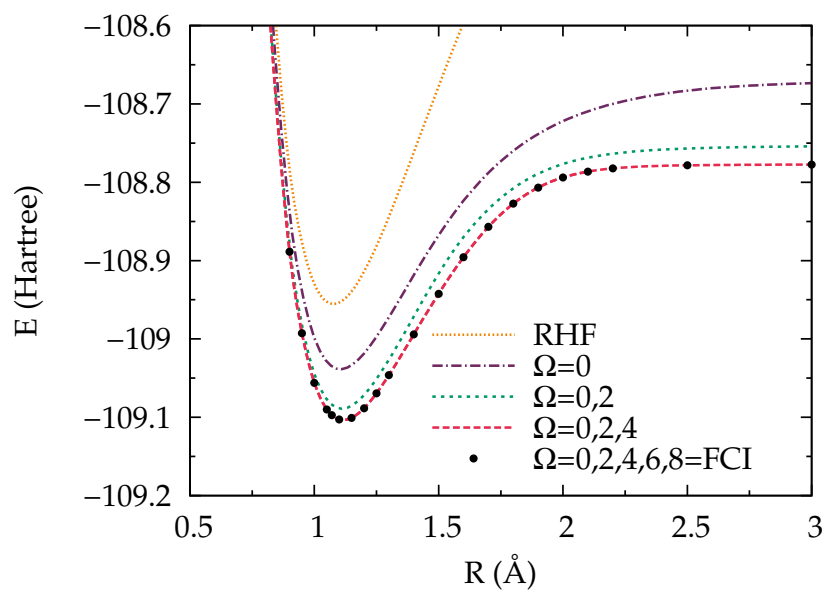
Figure 4.1.1 : Dissociation of N_2 molecule with seniority-based truncated configuration interaction with cc-pVDZ basis and minimal active space. Figure taken from Ref. [3].

of particle-hole excitations, *via* defining single excitations, double excitations *etc.* The reader may notice that this division is also not-unique and depends on the choice of reference state. The concept of excitation level is, however, crucial for truncation of the Hilbert space of the problem. Limiting the excitation levels present in the model is the heart of the truncated configuration interaction based methods and the coupled cluster methods. By analogy, the entire Hilbert space can be classified by a seniority number and then subjected to a suitable truncation. For example, by suitable choice of the paring scheme it is possible to diagonalize the Hamiltonian only in the space of seniority 0 determinants, seniority 0 and 2 determinants, and so on. The important feature of this truncation is that the convergence of the energy seems to be very rapid with the seniority number for strongly correlated systems. In other words, the exact ground state of the problem can be expressed in terms of determinants with low seniority number, provided an appropriate choice of pairing scheme can be found. [81] In Fig. 4.1.1, we show the dissociation of the nitrogen molecule computed by diagonalization of the Hamiltonian with a given level of the seniority truncation. As is clear, even with the retention solely of the seniority 0 determinants, the potential energy curve exhibits significant improvement over the uncorrelated HF description. The amount of correlation energy recovered, especially for the large bond lengths, suggests that the strong correlation is already well accounted for. Extending the model to larger seniorities brings the description of the missing correlation, yielding a quickly convergent expansion in Ω.

In the majority of the current chapter we therefore limit ourselves to the seniority 0 approximation. Diagonalizing the Hamiltonian in the $\Omega = 0$ space is known in the literature. [82–84] While called various names, we shall refer to this approximation as the doubly occupied configuration interaction (DOCI). Unfortunately, the DOCI,

though good at describing strong correlation, does not qualify as a computationally affordable tool. As opposed to truncation of the configuration expansion in the terms of particle-hole excitations, the seniority based approaches suffer from exponential scaling of the cost with the size of the problem. Therefore, the efforts of this work is to apply the concept of seniority to the coupled cluster methods.

4.2 Pair coupled cluster doubles

Formally, pair coupled cluster doubles does not differ significantly from the conventional CC approaches described in Section 3.4. The wavefunction ansatz takes the usual form

$$|\Psi\rangle = e^{\hat{T}}|0\rangle, \tag{4.2}$$

with $\hat{T}$ creating only double excitations. The difference is that not all double excitations are allowed. Only the excitation operators that do not change the seniority of the underlying determinant are included in the cluster operator. In other words,

$$\hat{T} = \sum_{ia} t_i^a \hat{P}_a^\dagger \hat{P}_i, \tag{4.3}$$

with $\hat{P}_p^\dagger = p_\uparrow^\dagger p_\downarrow^\dagger$ and, as usual, i (a) denoting a hole (particle) index. The rest of the approach follows directly. One defines a Lagrangian

$$\mathcal{L}(t, z) = \langle 0|(1 + \hat{Z})e^{-\hat{T}}He^{\hat{T}}|0\rangle, \tag{4.4}$$

with $\hat{Z} = \sum_{ia} z_a^i \hat{P}_i^\dagger \hat{P}_a$, and finds the t and z amplitudes by making the Lagrangian stationary. The resulting t equations take the form

$$2t_i^a(f_{ii} - f_{aa}) = v_{ii}^{aa} + v_{cc}^{aa}t_i^c + v_{ii}^{kk}t_k^a - 2t_i^a(2v_{ia}^{ia} - v_{ai}^{ia}) + t_k^a v_{cc}^{kk}t_i^c \tag{4.5}$$

$$- 2t_i^a(v_{cc}^{ii}t_i^c + v_{aa}^{kk}t_k^a) + 2t_i^a v_{aa}^{ii}t_i^a$$

and the z equations

$$0 = v_{aa}^{ii} + 2z_a^i(f_{aa} - f_{ii} - t_k^a v_{aa}^{kk} - t_i^c v_{cc}^{ii}) + z_a^k v_{kk}^{ii} + z_c^i v_{aa}^{cc} + t_k^c(z_a^k v_{cc}^{ii} + z_c^i v_{aa}^{kk}) \quad (4.6)$$

$$- 2v_{aa}^{ii}(z_a^k t_k^a + z_c^i t_i^c - 2z_a^i t_i^a) - 2z_a^i(2v_{ia}^{ia} - v_{ai}^{ia}).$$

As the reader may notice, the pair approximation yields a very simple set of equations which can be readily solved by an iterative approach with merely $\mathcal{O}(N^3)$ time. This should be compared with the $\mathcal{O}(N^6)$ time needed to solve the full CCD model. We note in passing that the pCCD is equivalent to the recently introduced AP1roG approach. [85–87]

Unfortunately, the above formalism is not sufficient to describe the strongly correlated systems with the pCCD approach. In order to have a complete model, an appropriate definition of the paring scheme must be provided. For the purpose of this work we augment the definition of the pCCD Lagrangian with a one-body antihermitian operator $\hat{\kappa}$,

$$\hat{\kappa} = \sum_{p>q} \sum_{\sigma} \kappa_{pq}(p_\sigma^\dagger q_\sigma - q_\sigma^\dagger p_\sigma), \quad (4.7)$$

as

$$\mathcal{L}(t, z, \kappa) = \langle 0|(1 + \hat{Z})e^{-\hat{T}}e^{-\hat{\kappa}}He^{\hat{\kappa}}e^{\hat{T}}|0\rangle. \quad (4.8)$$

We then require that

$$\left.\frac{\partial \mathcal{L}(t, z, \kappa)}{\partial \kappa_{pq}}\right|_{\kappa=0} = 0. \quad (4.9)$$

For simplicity, we always work with $\kappa = 0$ by iterative transformation of the basis in which we express the Hamiltonian. This allows us to recast the resulting orbital gradient and Hessian only in terms of the Hamiltonian matrix elements and the pCCD

density matrices,

$$\gamma_{pq} = \sum_{\sigma} \langle 0|(1 + \hat{Z})e^{-\hat{T}}q_{\sigma}^{\dagger}p_{\sigma}e^{\hat{T}}|0\rangle \tag{4.10}$$

$$\Gamma_{pqrs} = \sum_{\sigma\sigma'} \langle 0|(1 + \hat{Z})e^{-\hat{T}}r_{\sigma}^{\dagger}s_{\sigma'}^{\dagger}q_{\sigma'}p_{\sigma}e^{\hat{T}}|0\rangle \tag{4.11}$$

which can be constructed in a computationally efficient way as outlined in Ref. [3]. The above approach is analogous to the standard orbital optimization procedure in the CC methods, [88,89] with the only distinction that the hole-hole and particle-particle blocks must be considered, because unlike the standard CC approaches which depend only on the reference determinant, the pCCD depends also on the choice of orbitals in which said determinant is expressed. We have found that a simple Newton-Raphson algorithm is sufficient to converge most of the studied cases rather rapidly. In fact, a diagonal approximation to the Hessian seems to be sufficient for most situations.

4.3 Results

As was outlined so far, DOCI seems to be quite a robust method for capturing the majority of strong electron correlation. The usefulness of the pCCD approach could then be established by comparing the quality of the pCCD predictions against those of DOCI. In this section, we study a few potential energy surfaces for the dissociation process of small molecules where DOCI is feasible. Apart form looking at the correlation energy description, we shall also investigate the "closeness" of the pCCD eigenbra and eigenket to the corresponding DOCI states. In particular, we compute an overlap S

$$S = \langle 0|(1 + \hat{Z})e^{-\hat{T}}|\text{DOCI}\rangle\langle\text{DOCI}|e^{\hat{T}}|0\rangle, \tag{4.12}$$

We note that a value of S close to 1 would imply that the ground state DOCI state is well represented by the pCCD approach. One should, however, keep in mind that due to the biorthogonal framework employed in CC methods, the overlap need not be bound between 1 and 0. We posit, nonetheless, that an overlap close to 1 and good reproduction of the correlation energy allows one to conclude that physical predictions made with pCCD will closely mimic analogous predictions made with DOCI.

4.3.1 Hydrogen networks and lithium hydride

We start our investigations by examining a commonly employed prototypical system dominated by strong correlations, the hydrogen chains. In Fig. 4.3.1 we present the difference between the DOCI energy and pCCD energy evaluated in the orbitals optimized for the pCCD Lagragnian. As the reader may notice, during the course of symmetric dissociation of said system, the pCCD does not differ from DOCI significantly. The major discrepancy appears in the intermediate distances where the transition from molecular character to atomic character happens. This discrepancy is also visible by investigation of the overlap S. Clearly, a tiny deviation of this quantity from 1 is only visible in the intermediate coupling.

The remaining question is whether such good agreement between the pCCD and DOCI is just a feature for the optimized orbitals only. From our numerical experience we found that the optimal pCCD orbitals tend to be highly localized, forming effectively a set of weakly interacting electron pairs which are then treated very accurately by the pCCD ansatz. We have therefore performed analogous calculations employing de-localized HF canonical orbitals for the same systems. The results are presented in Fig. 4.3.2. We find that in this case the agreement between the DOCI and pCCD is less satisfactory, but the difference is not big.

Figure 4.3.1 : Dissociation of equally spaced hydrogen chains. The figure shows the difference between DOCI and pCCD energies (top panel) and the deviation of the overlap S (bottom panel). The calculations were performed with the cc-pVDZ basis and the orbitals were optimized with the pCCD Lagrangian. N denotes the number of electron pairs. Figure taken from Ref. [3].
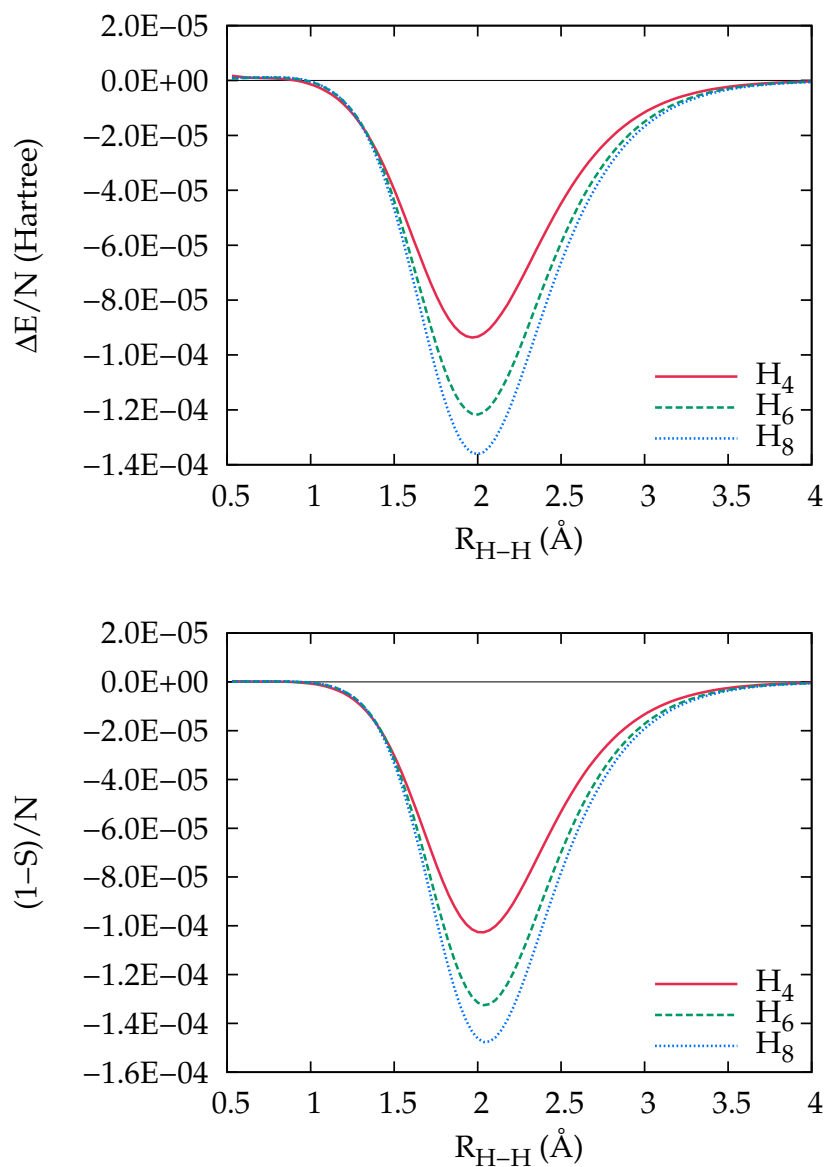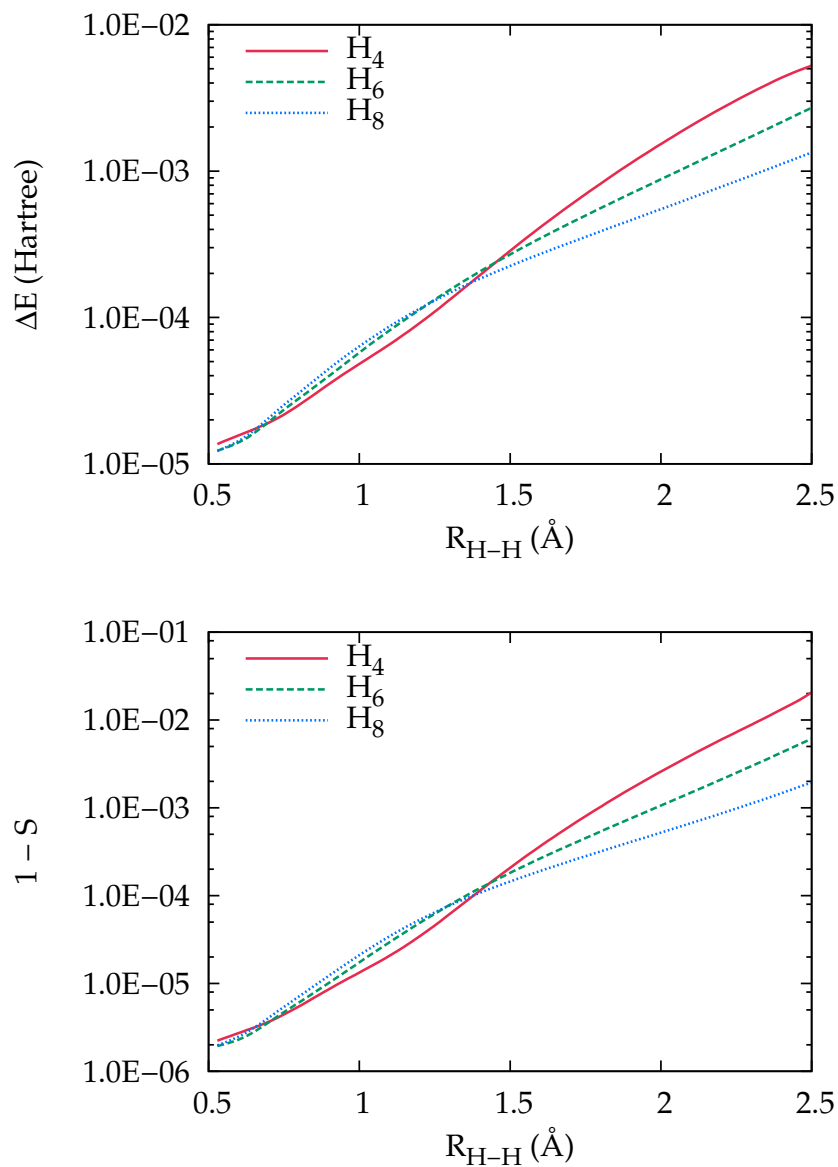
Figure 4.3.2 : Dissociation of equally spaced hydrogen chains. The figure shows the difference between DOCI and pCCD energies (top panel) and the deviation of the overlap S (bottom panel). The calculations were performed with the cc-pVDZ basis. The orbitals used were the canonical HF orbitals. Figure taken from Ref. [3].

Let us clarify the above statement that the pCCD ansatz tends to favour formation of weakly interacting electron pairs where the intrapair correlations are accounted for with high precision by the pCCD and DOCI approaches. To do so, we study the dissociation of LiH molecule. In this system, the 1s orbitals of lithium are relatively inactive and the physical description of the dissociation process requires us to account only for the LiH bonding pair. As exemplified in Fig. 4.3.3, the DOCI and pCCD for such systems agree perfectly with the exact solution (FCI). All three curves overlap perfectly in the potential energy profile and the overlap between the DOCI and pCCD states does not deviate significantly from unity.

4.3.2 Water and nitrogen molecules

Let us now turn our attention to slightly more challenging systems where the total correlation energy is not expressible as set of weakly interacting electron pairs. Here we study the symmetric dissociation of the water molecule and the nitrogen molecule.

For the case of water, the results are shown in Fig. 4.3.4. Here, we benchmark the DOCI/pCCD against unrestricted CCSD and CCSD(T). As the reader may notice, the pCCD/DOCI agreement holds equally well for the dissociation of the water molecule as in the simple examples of hydrogen chains. Nonetheless, restriction of the seniority sectors to $\Omega = 0$ clearly does not suffice to account well for the residual correlations around the equilibrium bond length. The important thing to keep in mind is that pCCD does account for strong correlation at the large bond distances. The resulting error may again be described by the tendency of pCCD to exhibit a perfect paring structure of the t amplitudes. In other words, the dominant configurations in the cluster operator correspond to individual couplings between the hydrogen-oxygen σ and $\sigma^\star$ orbitals. Of course, the pCCD ansatz is more flexible than the perfect paring
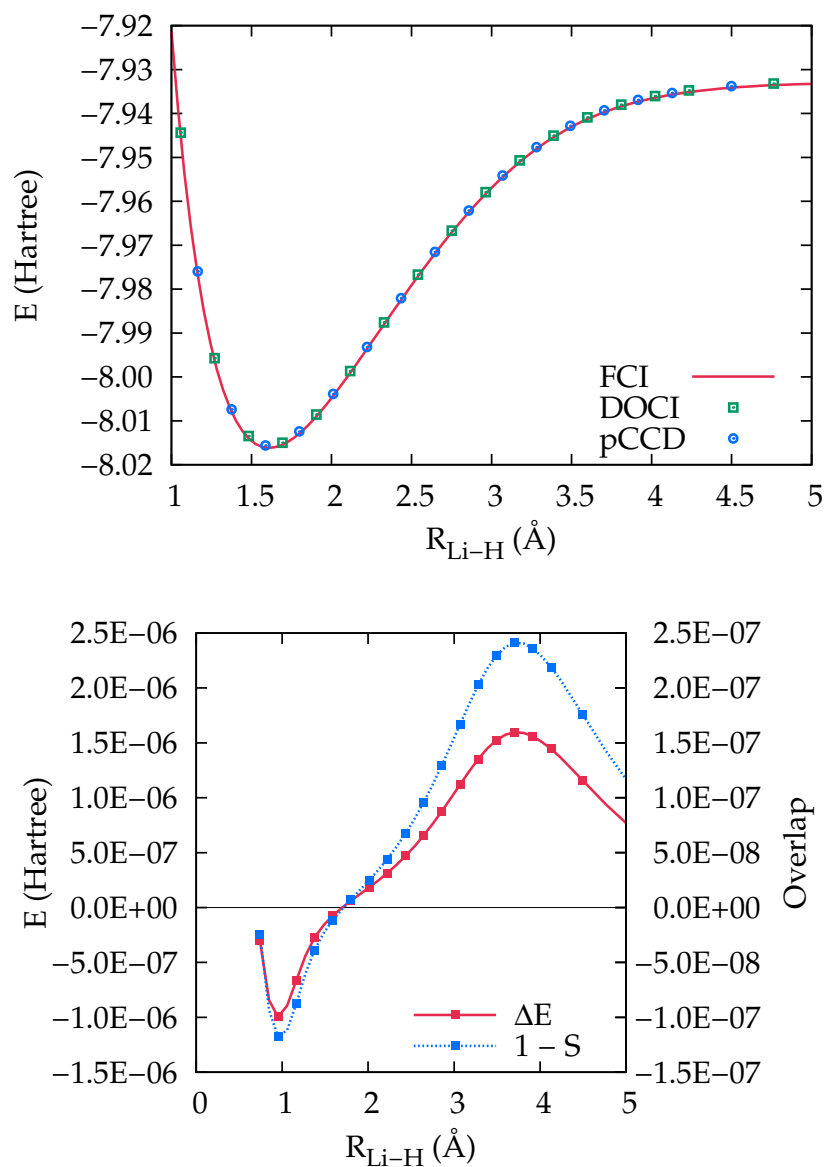
Figure 4.3.3 : Dissociation of lithium hydride. The figure shows the energy obtained with pCCD, DOCI and the exact one (FCI) within the cc-pVDZ basis employed (top panel), and the difference between DOCI and pCCD energies and the deviation of S from unity (bottom panel). The orbitals used for pCCD and DOCI were optimized with pCCD Lagrangian. Figure taken from Ref. [3].

approximation and some residual correlations are also accounted for.

Let us be more specific in what we mean by pCCD being able to account for strong correlation. In order to illustrate the point clearer, we present the nitrogen molecule dissociation curve in Fig. 4.3.5. In this case, apart from the unrestricted CCSD (UCCSD), we also include the restricted CCSD (RCCSD). As apparent from the figure, the RCCSD curve displays an unphysical behaviour where the potential energy exhibits a bump, after which the curve becomes dissociative. This behaviours is not, however, present in the DOCI and pCCD. Despite the fact that the over-all energy predicted by those methods are somehow underestimated, no qualitative breakdown of the approximations is visible. This observation is even more intriguing as the pCCD is just a simplification of the RCCSD. Indeed, the RCCSD includes de-terminants of higher seniority in the projective subspace. A more detailed discussion of this issue is presented in Section 4.4. Here, let us just notice that the unrestricted HF formalism provides a reasonable description of the N_2 energy over the entire dis-sociation curve and the CCSD approach based on this determinant does not exhibit any of the unphysical behaviour.

4.4   Why does pair coupled cluster work?

In the preceding sections we have outlined the formalism of the pair coupled cluster approach and benchmarked it on the examples of prototypical strongly correlated systems. Despite extensive efforts, we were unable to find a single example where the pCCD breaks down (for repulsive Hamiltonian), even though the standard CCSD and CCD models are known to fail catastrophically if based on restricted Hartree-Fock determinant in the cases where strong correlation is dominant. This could be clearly seen in the example of nitrogen molecule dissociation. In the present section, we try

Figure 4.3.4 : Symmetric dissociation of water molecule. The figure shows the energy obtained with pCCD, DOCI as well as standard CC approaches (top panel). The differences between the DOCI and pCCD are highlighted in the bottom panel. The calculations were done using cc-pVDZ basis. The orbitals for pCCD and DOCI were obtained by optimizing the pCCD Lagrangian. Figure taken from Ref. [3].
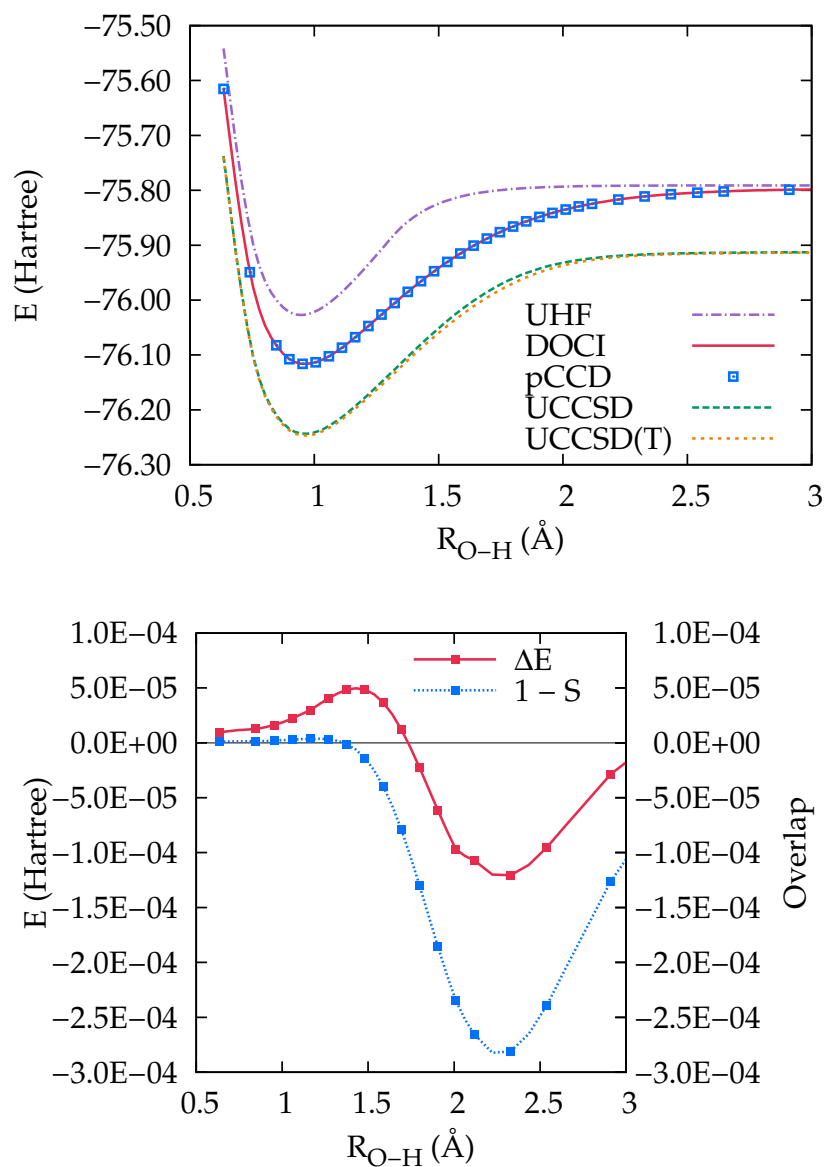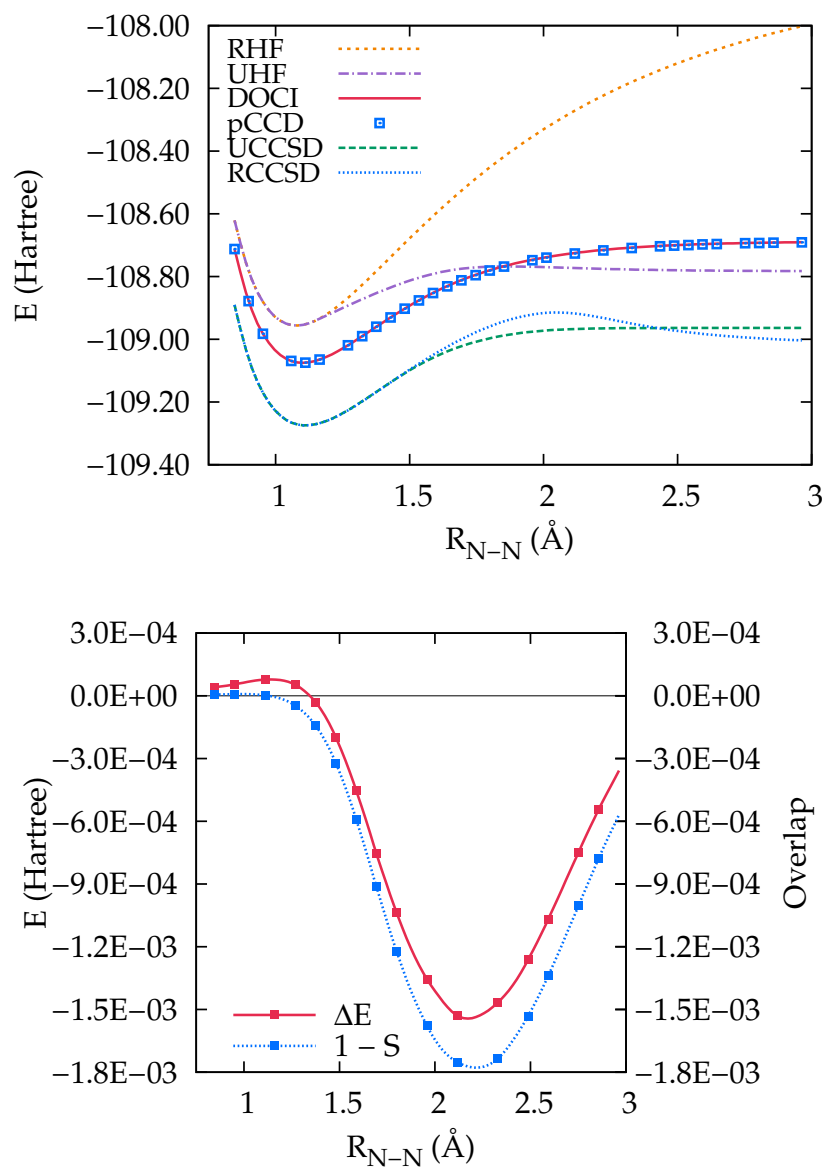
Figure 4.3.5 : Dissociation of nitrogen molecule. The figure shows the energy obtained with pCCD, DOCI as well as standard CC approaches (top panel). The differences between the DOCI and pCCD are highlighted in the bottom panel. The calculations were done using cc-pVDZ basis. The orbitals for pCCD and DOCI were obtained by optimizing pCCD Lagrangian. Figure taken from Ref. [3].

to understand the reason of such great robustness.

The most obvious feature of the pCCD is that the cluster operator cannot change the seniority of the reference determinant, i.e.

$$\hat{T} = \sum_{ia} t_i^a P_a^\dagger P_i. \tag{4.13}$$

The straightforward interpretation of the pCCD success in the strongly correlated system could therefore be attributed to this fact. Let us however suggest an alternative explanation that will result in formulation of a coupled cluster method that goes beyond the $\Omega = 0$ space of determinants while still exhibiting surprising robustness against catastrophic failures in the strong correlation regime.

In the commonly employed approach to derive a spin-restricted CCD equations, one starts by casting the cluster operator in terms of spin-symmetry adapted excitation operators $E_i^a = \sum_\sigma (a_\sigma^\dagger i_\sigma)$ [90] as

$$\hat{T}_2 = \frac{1}{2} \sum_{abij} t_{ij}^{ab} E_i^a E_j^b. \tag{4.14}$$

Let us now define a set of operators,

$$(P_{ab}^+)^\dagger = a_\alpha^\dagger b_\alpha^\dagger \tag{4.15}$$

$$(P_{ab}^-)^\dagger = a_\beta^\dagger b_\beta^\dagger \tag{4.16}$$

$$(P_{ab}^1)^\dagger = \frac{1}{\sqrt{2}}(a_\alpha^\dagger b_\beta^\dagger - b_\alpha^\dagger a_\beta^\dagger) \tag{4.17}$$

$$(P_{ab}^0)^\dagger = \frac{1}{\sqrt{2}}(a_\alpha^\dagger b_\beta^\dagger + b_\alpha^\dagger a_\beta^\dagger), \tag{4.18}$$

that creates pair of particles in states a and b and the corresponding pair-anihilation operators acting in the hole states. The operators can be classified as creators of triplet pairs with m_z component of $+1$, -1 and 0 for Eq. 4.15-4.17 and singlet pair for Eq. 4.18, respectively. Then, the cluster operator in the terms of the above

operators becomes,

$$\hat{T}_2 = \frac{1}{4}\sum_{abij} t^{a_\alpha b_\alpha}_{i_\alpha j_\alpha}(P^+_{ab})^\dagger P^+_{ij} + \frac{1}{4}\sum_{abij} t^{a_\beta b_\beta}_{i_\beta j_\beta}(P^-_{ab})^\dagger P^-_{ij} + \frac{1}{2}\sum_{abij} s^{ab}_{ij}(P^0_{ab})^\dagger P^0_{ij}$$

$$+ \frac{1}{2}\sum_{abij} a^{ab}_{ij}(P^1_{ab})^\dagger P^1_{ij}. \tag{4.19}$$

In the above expression, $s^{ab}_{ij} = \frac{1}{2}\left(t^{a_\alpha b_\beta}_{i_\alpha j_\beta} + t^{a_\alpha b_\beta}_{j_\alpha i_\beta}\right)$ and $a^{ab}_{ij} = \frac{1}{2}\left(t^{a_\alpha b_\beta}_{i_\alpha j_\beta} - t^{a_\alpha b_\beta}_{j_\alpha i_\beta}\right)$. As noted in Ref. [90], the spin adaptation of the cluster amplitudes poses constraints in the individual components of t, namely, $t^{a_\alpha b_\alpha}_{i_\alpha j_\alpha} = t^{a_\beta b_\beta}_{i_\beta j_\beta} = 2a^{ab}_{ij}$. Clearly, setting $a^{ab}_{ij} = 0$ and constraining the singlet paring operators to have only $a = b$ terms is equivalent to pCCD.

Guided by the exceptional robustness of pCCD we proceed to investigate whether a generalization of pCCD to include electron correlation beyond the $\Omega = 0$ sector is possible. To that extent, we implemented the constrained coupled cluster where the cluster operator takes the form

$$\hat{T}_2 = \frac{1}{2}\sum_{abij} s^{ab}_{ij}(P^o_{ab})^\dagger P^o_{ij} = \hat{\sigma}. \tag{4.20}$$

We denote this cluster operator as σ and refer to the coupled cluster approach with said operator as CCD0, as it comes from excitation operators composed of singlet paring operators. Alternatively, one may also define the operator

$$\hat{T}_2 = \frac{1}{4}\sum_{abij} t^{a_\alpha b_\alpha}_{i_\alpha j_\alpha}(P^+_{ab})^\dagger P^+_{ij} + \frac{1}{4}\sum_{abij} t^{a_\beta b_\beta}_{i_\beta j_\beta}(P^-_{ab})^\dagger P^-_{ij} + \frac{1}{2}\sum_{abij} a^{ab}_{ij}(P^1_{ab})^\dagger P^1_{ij} = \hat{\pi}, \tag{4.21}$$

which is composed of the triplet paring operators.

At this stage, let us comment on the physical intuition underlying the above development. Let us begin with an established connection between the random phase approximation (RPA) and the coupled cluster approaches, namely, coupled cluster doubles can be simplified to be equivalent to RPA. [91–93] It is well known that

RPA breaks down (i.e. the correlation energy may become complex), whenever a restricted HF approach becomes unstable towards spin symmetry breaking. [94, 95] This is an indication of strong electron correlation. While by including all the terms in coupled cluster breaks the explicit connection with the RPA, we numerically verify that the removal of the RPA parts cures the instabilities. In particular, removing just the quadratic RPA terms in the amplitudes equations can alleviate that problem as well. On the other hand, pair coupled cluster does include all of the terms. Guided by that insight we proceed to investigate whether the coupling between the σ and π amplitudes in the quadratic terms could be part of the instability problem in coupled cluster. Unfortunately, removing only parts of the coupled cluster equations means that one no longer has a well defined ansatz that diagonalizes a Hamiltonian in the projective subspace. On the other hand, forming an ansatz that prevents the coupled cluster from breaking down retains all the formally pleasing properties of the traditional coupled cluster approach.

As pCCD is just an approximation to CCD0, we think that the incredible robustness of pair coupled cluster doubles does not need to be fully accounted for by the seniority argument. As we show in the following section, CCD0 displays no instabilities while describing the dissociation of molecules, a typical example of strong correlation, despite including all seniority determinants in the expansion. Therefore, the description of the electron correlation is more accurate. Moreover, the invariance with respect to particle-particle and hole-hole mixing is restored, rendering the orbital optimization not crucial. Nonetheless, the computational scaling of pCCD remains lower than CCD0.
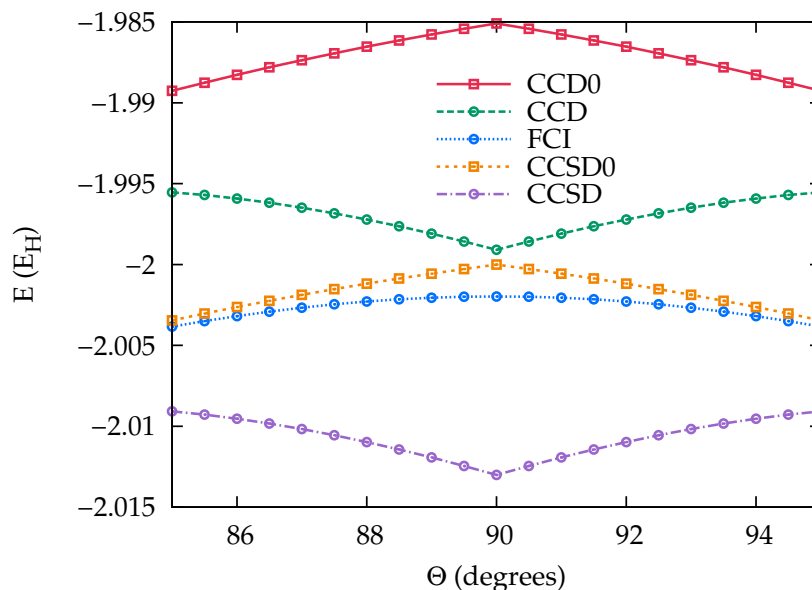
Figure 4.4.1 : Total energy of H_4 on a ring (see text for details). The FCI data and the basis set is adapted from Ref. [4]. Figure taken from Ref. [5].

4.4.1   CCD0: benchmark calculations

Let us start by a simple model of strongly correlated system where the restricted coupled cluster fails miserably. We consider a system of 4 hydrogen atoms located on a ring of a radius 1.738 Å such that the angle between adjacent hydrogen pairs is Θ and $\pi - \Theta$. If the value of the angle Θ is small, then the system is represented by two separate hydrogen molecules, whereas as the angle approaches $\frac{\pi}{2}$, the atoms form a square and individual molecules cannot be meaningfully defined. We now ask the question, what is the most stable arrangement of that system? The results of the calculations are shown in Fig. 4.4.1. The data compares CCD with CCD0 and CCSD with CCSD0. The exact results are included for comparison. Clearly, both, CCD and CCSD methods predict that the square is the most stable arrangement,

which is somehow counterintuitive from the chemical point of view. By constraining the $\hat{T}_2$ cluster operator to be composed of the singlet-paring operators the results are completely different. In agreement with the exact answer (FCI), CCSD0 and CCD0 identify the square arrangement as the most unstable. Nonetheless, the exact answer provides a smooth curve over the entire range of the Θ angle studied while CCSD0 and CCD0 include a nonphysical kink. This kink was also observed in other approaches aiming to amend coupled cluster theory. [4]

Let us now move to another prototypical example of system where the CCSD based on restricted Hartree-Fock reference breaks down, the N_2 molecule, as shown in Fig. 4.4.2. In this case, we have extended the cluster operator to also include triple excitations, CCSDT. The results where the $\hat{T}_2$ operator is composed of only the singlet paring channel and triple excitations are included is denoted as CCSDT0. Once again, we observe that the equations with the full set of the amplitudes leads to unphysical barriers of bond formation. On the other hand, the singlet-only approximation yields curves that are smooth and do not have unphysical features. Nonetheless, CCSD0 and CCSDT0 are not a ultimate solution. Clearly, both methods miss significant amount of correlation at the equilibrium geometry and dissociation limit.

4.4.2 CCD1: another stable channel ?

So far, guided by the pCCD approach we suggested an extension to this model in the form of CCD0. Just as in pCCD, we observe significant robustness of this approximation in the strongly correlated regime. The reader may be then curious whether the second part of the cluster operator, $\hat{\pi}$ of Eq. 4.21 is the reason of the instabilities of coupled cluster. The results of the calculations, labeled CCD1, are presented in Fig. 4.4.3 for the case of nitrogen molecule. Please note that here we used a smaller basis

Figure 4.4.2 : Potential energy profile for N_2 molecule with cc-pVDZ basis, evaluated with different coupled cluster schemes (see text for details). Figure taken from Ref. [5].

set in which the failure of traditional coupled cluster is more visible. Clearly, CCD1 and CCD0 are both separately stable. The amount of correlation provided by CCD0 is significantly larger. This can be understood by the same-spin (provided by CCD0) and opposite-spin correlation (provided by CCD1) effects. In other words, much of the same-spin interaction is already taken into accounted by *via* exchange.

4.4.3 CCD0 and CCD1: insights

How can one make sense of the results presented here? Pair coupled cluster, as far as our numerical results suggest, is an unbreakable approximation for repulsive Hamiltonians. The seniority arguments, though, may not be the only reason for its stability. Both, CCD0 and CCD1 seems to be stable for molecular systems as

well, even though both include higher seniorities whereas the latter does not contain seniority zero. Nonetheless, keeping both $\hat{\sigma}$ and $\hat{\pi}$ parts of the cluster operator leads to unstable results. It would then seem that allowing for the cross terms between those operators may be the culprit though removing simply those terms requires one to sacrifice the wavefunction.

We do not claim that CCD0 and CCD1 are valuable computational tools by themselves. On the contrary; one should put the missing bits of the correlation back into CCD0. We just point out that this has to be done with care in order not to introduce the original instabilities. Clearly, the CCD0 approach falls into a category of improvement by simplification, just like pCCD. While there were many studies that tried to amend coupled cluster my making it more complete [4, 96] the alternative outlined here did not receive much attention. Successful approaches have been reported [97–99] yet those would fall into category of modifying the resulting CCD equations not the CCD ansatz.

4.5   Conclusion

In the present section we introduced the idea of seniority and explained how it can be applied to simplify the coupled cluster approaches. We outlined pair coupled cluster doubles and benchmarked it for typical bond breaking processes. The method turned out to provide a satisfactory description of strong correlation with a low computational cost. Strikingly, we found numerical evidence that pCCD reproduces extremely well DOCI, where DOCI is the limit of the accuracy in the $\Omega = 0$ sector. In other words, by including higher and higher excitations operators into the cluster operator we are bound to converge to the DOCI limit. While the latter has an exponential computational scaling, pCCD seems to provide an excellent polynomial parametrization
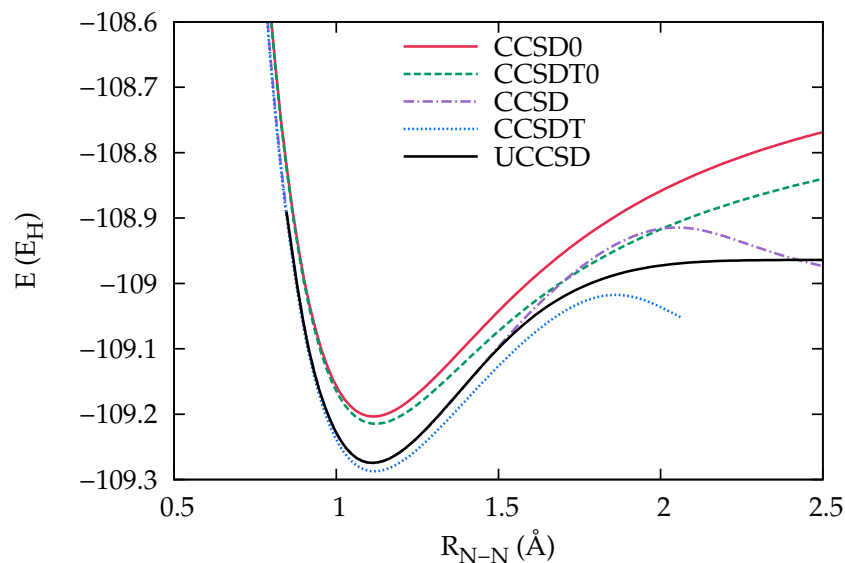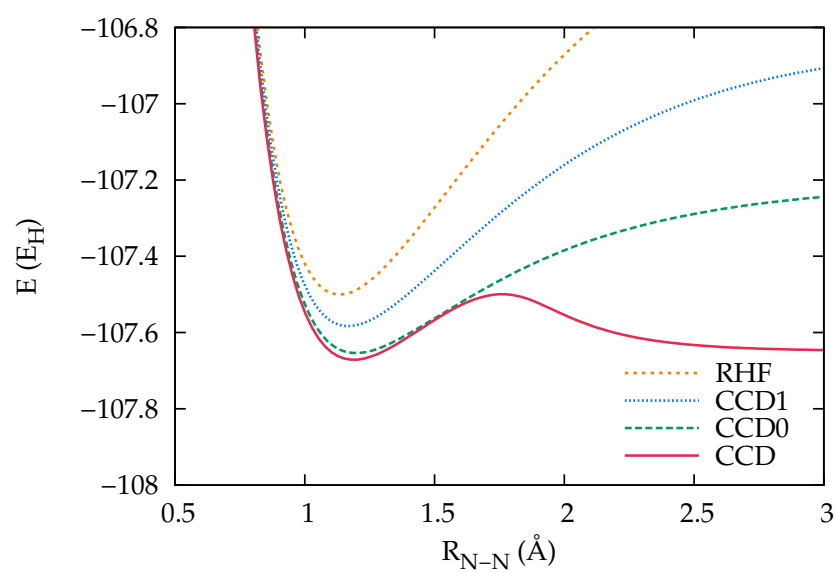
Figure 4.4.3 : Potential energy profile for N_2 molecule with the STO-3G basis, evaluated with different coupled cluster schemes (see text for details). Figure taken from Ref. [5].

of this wavefunction, at least in the repulsive Hamiltonians.

As the density matrices are readily available, the methods seems to be well suited for large scale impurity problems in the DMET embedding. Nonetheless, it can also serve as a viable stand-alone quantum-chemical tool or in combination with other standard approaches as the density functional theory. Indeed, we tried to account for the missing correlation effect by combination of pCCD with DFT with promising results [100].

While trying to understand the robustness of pCCD, we were able to provide its generalization to higher seniority sectors that retains a good behaviour in the strongly correlated limit when the standard coupled cluster breaks. With slight increase of the computational cost, we were able to account for higher seniority determinants in the projective space of the coupled cluster. Of course, neither pCCD nor CCD0 are capable of accounting for all of the electron correlation. Nonetheless, we believe that both methods are a good starting point for suggesting more elaborate many-body theories.

Chapter 5

Conclusions

In the present thesis we tried to contribute to the collective efforts towards accurate description of electron correlation. In particular, we aimed to develop and benchmark quantum embedding theory. From that perspective, we studied the density matrix embedding theory as a tool for truncating the dimension of the many-body Hilbert space by defining locally important single particle degrees of freedom. We were guided by a desire of developing easy-to-use and computationally efficient theories that are benchmarked against accurate reference data. In that respect, we investigated the performance of the embedding approach for model systems where exact results are known and found satisfactory performance. We then proceeded to apply this theory for model chemical systems with an approximate method to solve the resulting impurity problem. Again, the data suggest that DMET works very well, even though it significantly reduces the dimension of the Hilbert space. Finally, we discuss and present a computationally efficient many-body theory that can be considered as an impurity solver for the systems where strong electron correlation may be important and the size of the fragment is sufficiently large that exact of very accurate approaches are computationally intractable.

Some of the problems treated in the present thesis are not fully resolved. A more extensive benchmark for the embedding procedure is clearly called for. The tools required to perform the calculations are available and can be employed in further studies. The pair coupled cluster approach may be further improved by combination

of this ansatz with other many-body approaches. At the point of submitting this thesis, the author have combined pCCD with other similarity transformation based methods and applied it to model systems. Finally, the CCD0 approach outlined here needs to be further investigated. Again, initial trials of accounting for missing electronic correlations were attempted but not included in the present thesis.

Bibliography

[1] I. W. Bulik, G. E. Scuseria, and J. Dukelsky, Phys. Rev. B **89**, 035140 (2014).

[2] I. W. Bulik, W. Chen, and G. E. Scuseria, J. Chem. Phys **141**, 054113 (2014).

[3] T. M. Henderson, I. W. Bulik, T. Stein, and G. E. Scuseria, J. Chem. Phys **141**, 244104 (2014).

[4] T. Van Voorhis and M. Head-Gordon, J. Chem. Phys **113**, 8873 (2000).

[5] I. W. Bulik, T. H. Henderson, and G. E. Scuseria, submitted (2015).

[6] A. Szabo and S. Ostlund, Neil, *Modern Quantum Chemistry* (Dover Publications, Inc., Mineola, N.Y., 1996).

[7] P. Ring and P. Schuck, *The nuclear many-body problem* (Springer, Berlin, 2005).

[8] K. Raghavachari and J. B. Anderson, J. Phys. Chem. **100**, 12960 (1996).

[9] K. Jankowski, in *Methods in Computational Chemistry*, edited by S. Wilson (Springer US, ADDRESS, 1987), pp. 1–116.

[10] H.-J. Werner and W. Meyer, Phys. Rev. A **13**, 13 (1976).

[11] T. Helgaker, P. Jorgensen, and J. Olsen, *Molecular electronic-structure theory* (John Wiley & Sons, ADDRESS, 2014).

[12] A. P. Scott and L. Radom, J. Phys. Chem. **100**, 16502 (1996).

[13] A. M. Lesk, J. Chem. Phys **59**, 44 (1973).

[14] V. K. Voora, L. S. Cederbaum, and K. D. Jordan, J. Phys. Chem. Letters **4**, 849 (2013).

[15] M. Imada, A. Fujimori, and Y. Tokura, Rev. Mod. Phys. **70**, 1039 (1998).

[16] G. Kotliar and D. Vollhardt, Physics Today **57**, 53 (2004).

[17] M. J. Frisch, Reflections on Jhon Pople's Career and Legacy, 2004, http://www.gaussian.com/g_people/pople.htm, accessed April, 2015.

[18] F. Coester, Nucl. Phys. **7**, 421 (1958).

[19] F. Coester and H. Kümmel, Nucl. Phys. **17**, 477 (1960).

[20] J. A. Pople, R. Krishnan, H. B. Schlegel, and J. S. Binkley, Int. J. Quantum Chem. **14**, 545 (1978).

[21] R. J. Bartlett and G. D. Purvis, Int. J. Quantum Chem. **14**, 561 (1978).

[22] G. E. Scuseria *et al.*, J. Chem. Phys **86**, 2881 (1987).

[23] G. E. Scuseria and H. F. Schaefer, J. Chem. Phys **90**, 3700 (1989).

[24] T. D. Crawford and H. F. Schaefer, in *Reviews in Computational Chemistry* (John Wiley & Sons, Inc., ADDRESS, 2007), pp. 33–136.

[25] R. J. Bartlett and M. Musiał, Rev. Mod. Phys. **79**, 291 (2007).

[26] J. Noga and R. J. Bartlett, J. Chem. Phys **86**, 7041 (1987).

[27] G. E. Scuseria and H. F. S. III, Chem. Phys. Lett. **152**, 382 (1988).

[28] D. Hegarty and M. A. Robb, Mol. Phys. **38**, 1795 (1979).

[29] M. Frisch, I. N. Ragazos, M. A. Robb, and H. B. Schlegel, Chem. Phys. Lett. **189**, 524 (1992).

[30] R. H. Eade and M. A. Robb, Chem. Phys. Lett. **83**, 362 (1981).

[31] G. E. Scuseria *et al.*, J. Chem. Phys **135**, 124108 (2011).

[32] C. A. Jiménez-Hoyos, T. M. Henderson, T. Tsuchimochi, and G. E. Scuseria, J. Chem. Phys **136**, 164109 (2012).

[33] R. Rodríguez-Guzmán, K. W. Schmid, C. A. Jiménez-Hoyos, and G. E. Scuseria, Phys. Rev. B **85**, 245130 (2012).

[34] L. Piela, *Ideas of Quantum Chemistry* (Elsevier, Amsterdam, 2007).

[35] E. Engel and R. M. Dreizler, *Density Functional Theory: An Advanced Course* (Springer-Verlag, Berlin Heidelberg, 2011).

[36] G. E. Scuseria and V. N. Staroverov, in *Theory and Applications of Computational Chemistry*, edited by C. E. Dykstra, G. Frenking, K. S. Kim, and G. E. Scuseria (Elsevier, Amsterdam, 2005), pp. 669 – 724.

[37] K. Burke, J. Chem. Phys **136**, 150901 (2012).

[38] G. Knizia and G. K.-L. Chan, Phys. Rev. Lett. **109**, 186404 (2012).

[39] G. Knizia and G. K.-L. Chan, J. Chem. Theory Comput. **9**, 1428 (2013).

[40] I. Peschel, Braz. J. Phys. **42**, 267 (2012).

[41] I. Klich, J. Phys. A: Math. Gen. **39**, L85 (2006).

[42] E. H. Lieb and F. Y. Wu, Phys. Rev. Lett. **20**, 1445 (1968).

[43] V. L. Campo and K. Capelle, Phys. Rev. A **72**, 061602 (2005).

[44] A. Snyder, I. Tanabe, and T. De Silva, Phys. Rev. A **83**, 063632 (2011).

[45] N. A. Lima, M. F. Silva, L. N. Oliveira, and K. Capelle, Phys. Rev. Lett. **90**, 146402 (2003).

[46] G. Sordi, K. Haule, and A.-M. S. Tremblay, Phys. Rev. Lett. **104**, 226402 (2010).

[47] S. Hirata, J. Chem. Phys. **129**, 204104 (2008).

[48] T. Shimazaki and Y. Asai, J. Chem. Phys. **130**, 164702 (2009).

[49] E. Voloshina and B. Paulus, J. Chem. Theory Comput. **10**, 1698 (2014).

[50] G. H. Booth, A. Grüneis, G. Kresse, and A. Alavi, Nature **493**, 365 (2013).

[51] J. Heyd, J. E. Peralta, G. E. Scuseria, and R. L. Martin, J. Chem. Phys. **123**, 174101 (2005).

[52] M. J. Lucero, T. M. Henderson, and G. E. Scuseria, J. Phys.: Condens. Matter **24**, 145504 (2012).

[53] J. P. Perdew *et al.*, Phys. Rev. Lett. **100**, 136406 (2008).

[54] A. J. Cohen, P. Mori-Sánchez, and W. Yang, Science **321**, 792 (2008).

[55] I. W. Bulik, G. Scalmani, M. J. Frisch, and G. E. Scuseria, Phys. Rev. B **87**, 035117 (2013).

[56] H. Stoll, J. Chem. Phys. **97**, 8449 (1992).

[57] H. Stoll, Chem. Phys. Lett. **191**, 548 (1992).

[58] B. Paulus, Phys. Rep. **428**, 1 (2006).

[59] S. Suhai, Phys. Rev. B **50**, 14791 (1994).

[60] S. Suhai, Phys. Rev. B **51**, 16553 (1995).

[61] J. Sun and R. J. Bartlett, J. Chem. Phys. **104**, 8553 (1996).

[62] S. Hirata and S. Iwata, J. Chem. Phys. **109**, 4147 (1998).

[63] P. Y. Ayala, K. N. Kudin, and G. E. Scuseria, J. Chem. Phys. **115**, 9698 (2001).

[64] Y.-J. Ye, W. Förner, and J. Ladik, Chem. Phys. **178**, 1 (1993).

[65] P. Reinhardt, Theor. Chem. Acc. **104**, 426 (2000).

[66] S. Hirata, R. Podeszwa, M. Tobita, and R. J. Bartlett, J. Chem. Phys. **120**, 2581 (2004).

[67] N. Marzari *et al.*, Rev. Mod. Phys. **84**, 1419 (2012).

[68] J. Pipek and P. G. Mezey, J. Chem. Phys. **90**, 4916 (1989).

[69] P. Löwdin, J. Chem. Phys. **18**, 365 (1950).

[70] C. E. Pisani, *Quantum-Mechanical Ab-initio Calculation of the Properties of Crystalline Materials*, *Lecture Notes in Chemistry* (Springer-Verlag Berlin Hpageselberg New York, ADDRESS, 1996).

[71] J. F. Stanton, J. Chem. Phys. **99**, 8840 (1993).

[72] J. F. Stanton, J. Chem. Phys **101**, 371 (1994).

[73] J. Gauss and J. F. Stanton, J. Chem. Phys **103**, 3561 (1995).

[74] M. J. Frisch *et al.*, Gaussian Developement Version Revision H.21, gaussian Inc. Wallingford CT 212.

[75] R. Dovesi, C. Pisani, C. Roetti, and V. R. Saunders, Phys. Rev. B **28**, 5781 (1983).

[76] W. J. Hehre, R. Ditchfield, and J. A. Pople, J. Chem. Phys. **56**, 2257 (1972).

[77] J. D. Dill and J. A. Pople, J. Chem. Phys. **62**, 2921 (1975).

[78] L. Liu *et al.*, Science **343**, 163 (2014).

[79] C. Oshima and A. Nagashima, J. Phys.: Condens. Matter **9**, 1 (1997).

[80] Y. Andreev and T. Lundstrm, J. Alloy. Comp. **216**, L5 (1994).

[81] L. Bytautas *et al.*, J. Chem. Phys **135**, 044119 (2011).

[82] D. W. Smith and S. J. Fogel, J. Chem. Phys **43**, S91 (1965).

[83] C. Kollmar and B. A. Heß, J. Chem. Phys **119**, 4655 (2003).

[84] M. Couty and M. B. Hall, J. Phys. Chem. A **101**, 6936 (1997).

[85] P. A. Limacher *et al.*, J. Chem. Theory Comput. **9**, 1394 (2013).

[86] K. Boguslawski *et al.*, Phys. Rev. B **89**, 201106 (2014).

[87] P. A. Limacher *et al.*, Phys. Chem. Chem. Phys. **16**, 5061 (2014).

[88] G. E. Scuseria and H. F. S. III, Chem. Phys. Lett. **142**, 354 (1987).

[89] U. Bozkaya *et al.*, J. Chem. Phys **135**, 104103 (2011).

[90] G. E. Scuseria, C. L. Janssen, and H. F. Schaefer, J. Chem. Phys **89**, 7382 (1988).

[91] G. E. Scuseria, T. M. Henderson, and D. C. Sorensen, J. Chem. Phys **129**, 231101 (2008).

[92] G. E. Scuseria, T. M. Henderson, and I. W. Bulik, J. Chem. Phys **139**, 104113 (2013).

[93] D. Peng, S. N. Steinmann, H. van Aggelen, and W. Yang, J. Chem. Phys **139**, 104112 (2013).

[94] D. Thouless, Nuclear Physics **21**, 225 (1960).

[95] D. Thouless, Nuclear Physics **22**, 78 (1961).

[96] E. F. C. Byrd, T. Van Voorhis, and M. Head-Gordon, J. Phys. Chem. B **106**, 8070 (2002).

[97] D. Kats and F. R. Manby, J. Chem. Phys. **139**, (2013).

[98] P. Piecuch and J. Paldus, Int. J. Quantum Chem. **36**, 429 (1989).

[99] P. Piecuch and J. Paldus, Theor. Chimi. Acta **78**, 65 (1990).

[100] A. J. Garza, I. W. Bulik, T. M. Henderson, and G. E. Scuseria, J. Chem. Phys **142**, 044109 (2015).